Tsunami Inundation Variability from Stochastic Rupture Scenarios: Application to the 2011 Tohoku, Japan Earthquake Multiple Inversions

Nobuhito Mori[1], P. Martin Mai[2], Katsuichiro Goda[3], and Tomohiro Yasuda[4]

[1]Disaster Prevention Research Institute, Kyoto University, Japan

[2]Earth Science & Engineering, King Abdullah University of Science & Technology, Saudi Arabia

[3]Civil Engineering, University of Bristol, United Kingdom

[4]Environmental and Urban Engineering, Kansai University, Japan

Submitted to

Coastal Engineering

Corresponding author:

Nobuhito Mori

E-mail: mori.nobuhito.8a@kyoto-u.ac.jp

Abstract

We develop a framework for assessing the sensitivity and variability of tsunami inundation characteristics for stochastic physics-based scenarios of mega-thrust subduction earthquakes. The method is applied to the 2011 Tohoku, Japan earthquake, and tested against observed inundation maps at several locations along the Tohoku coast, using 11 different, previously published, rupture models for this devastating tsunamgenic earthquake. The earthquake rupture models differ in fault dimension (length and width), geometry (dip, strike and top-edge depth), as well as asperity characteristics (slip heterogeneity on the fault plane). The resulting source variability allows exploring a wide range of tsunami scenarios for an M_w9 mega-thrust subduction earthquake in the Tohoku region to conduct thorough sensitivity analyses and to quantify the inundation variability. The numerical results indicate a strong influence of the reference source models on inundation variability, and demonstrate significant sensitivity of inundation to the details of the rupture realization. Therefore, relying on a single particular earthquake rupture model as a representative case when varying earthquake source characteristics may lead to under-representation of the variability of potential scenarios. Moreover, the proposed framework facilitates the rigorous development of critical scenarios for tsunami hazard and risk assessments, which are particularly useful for tsunami hazard mapping and disaster preparedness planning.

Keywords: Tsunami simulation, 2011 Tohoku earthquake, Inundation mapping, Stochastic earthquake slip, Sensitivity analysis, Epistemic uncertainty

1 Introduction

The current state-of-the-practice for tsunami hazard mapping for coastal communities mainly considers tsunami hazard parameters (e.g. inundation depths and arrival times of major tsunami waves) that correspond to a single or at most a few scenarios on a selected fault. This approach lacks comprehensive information on the uncertainty of these hazard predictions. Consequently, the range of inundated areas and required structural design criteria cannot be adequately quantified, which in turn hampers the risk communications between tsunami analysts and local stakeholders. Therefore, users of scenario-based tsunami hazard maps may not be able to appreciate the potential risks (and their uncertainties) under different conditions. For instance, during the 2011 Tohoku, Japan tsunami, more than 65% of all fatalities in Kamaishi, Iwate Prefecture were caused outside the regions designated as major inundation zones in public tsunami hazard maps identified prior to 2005. The actual 2011 tsunami was beyond any historical events/scenarios considered for preparing the 2005 hazard map along the Sanriku and Sendai coasts. Clearly, a set of tsunami inundation hazard maps for coastal communities, corresponding to different tsunami scenarios and their consequences, is critically important for adequate tsunami hazard preparedness and evacuation planning. Using probabilistic hazard maps helps account for the main sources of uncertainty related to the tsunami characteristics, and promotes an informed decision-making for tsunami risk reduction by quantifying and understanding the consequences of different conditions and by communicating the uncertainty of hazard predictions (Pang, 2008).

One of the major challenges for tsunami impact assessment is to predict the earthquake source characteristics of future tsunamigenic events (e.g. location, magnitude, and slip distribution), and to then quantify the uncertainty associated with the variability in earthquake rupture and wave propagation/inundation processes (e.g. Burbidge et al., 2015). In particular, tsunami propagation and inland inundation characteristics are greatly influenced by complex and nonlinear interaction of earthquake source properties and changes in bathymetry and land elevation (Geist, 2002; McCloskey et al., 2008; Løvholt et al., 2012; Goda et al., 2014). Probabilistic tsunami hazard

analysis (Geist and Parsons, 2006; Thio et al., 2007; Gonzalez et al., 2009; Horspool et al., 2014; Fukutani et al., 2015; Mueller et al., 2015; Park et al., 2016), is a viable approach to identify tsunami source regions and corresponding scenarios that have major impact to a site of interest. Recently, the American Society of Civil Engineers (ASCE) has announced the new chapter 6 (6.7 *Inundation Depth and Flow Velocity Based on Site-Specific Probabilistic Tsunami Hazard Analysis*) to introduce design requirements for tsunami loads and effects (Chock, 2016) that can be defined through probabilistic tsunami hazard analysis. Therefore, the role of probabilistic tsunami hazard analysis becomes more important in both scientific and engineering fields. When developing critical design scenarios at a specific site, several experts are involved, each with different backgrounds and scientific views, leading to very diverse opinions on potential source characteristics. Such expert judgements rarely result in a consensus model, but rather generate a set of disparate scenarios that need to be weighted in a logic-tree approach (e.g. Fukutani et al, 2015).

Recent development in probabilistic tsunami hazard assessment facilitates the generation of stochastic earthquake source models based on an inverted slip distribution (Mai and Beroza, 2002; Lavallée et al., 2006; Goda et al., 2014, 2015a; Mori et al., 2017). These source models represent possible rupture scenarios having different earthquake slip and fault geometry. Because they are generated semi-automatically within a range of plausible, geophysically constrained parameter choices, they do not require expert judgment. The stochastic method is based on a wave-number domain analysis of slip heterogeneity of inverted rupture models, and implements a spectral random-phase approach to generate slip fields that capture realistic earthquake slip characteristics (i.e. distribution of high slip regions over the fault plane). This procedure allows generating an arbitrary number of synthetic slip models for a range of fault geometries and other source characteristics (e.g. length and width of fault, spectral shape of slip, and ratio of maximum and mean). For example, Goda et al. (2014, 2015a) developed a stochastic earthquake source generation approach for tsunami impact assessment based on an observed rupture model, while Goda et al. (2015b) have extended it to probabilistic tsunami damage assessment. However, their method used

95 a single inverted source model and did not consider the uncertainty in source parameter estimation,
96 as for instance documented in the variations of macroscopic source characteristics of published
97 earthquake rupture models (e.g. Mai and Thingbaijam, 2014). Obviously, it is imperative to
98 consider multiple inversion models to adequately evaluate the tsunami inundation and run-up as
99 well as their variability (MacInnes et al., 2013; Goda et al., 2014, 2015a).

100 The procedure of stochastic tsunami assessment is useful for assessing the sensitivity and
101 variability of tsunami hazard parameters by propagating the uncertainty associated with tsunami
102 sources from off-shore source regions to inland coastal regions by computing the complete
103 nonlinear fluid-dynamic response of the tsunami. By conducting Monte-Carlo type tsunami
104 simulations based on numerous source models, stochastic inundation depth maps can be generated
105 and then analyzed. Such a stochastic approach for tsunami scenario generation can be easily
106 incorporated into probabilistic tsunami hazard analysis. However, stochastic tsunami assessment
107 strongly depends on observations or historical events to make scenarios or synthetic slips. Therefore,
108 it is important to discuss influence of basic observations or historical events on outcomes (e.g.
109 inundation mapping).

110 This study investigates the sensitivity and variability of the spatial extent and depth of
111 tsunami inundation considering variations in fault geometry and slip distribution using stochastic
112 rupture models. The stochastic earthquake source realizations are calibrated using multiple results
113 of source inversion. The investigation focuses on the 2011 Tohoku event, because numerous
114 tsunami, seismic, and geodetic observations are available to validate the outcome of the tsunami
115 hazard assessment. Recognizing that different inversion models may reflect different aspects of the
116 earthquake rupture processes, a set of earthquake rupture models (developed by different
117 researchers using different methods and data) can be adopted to characterize parts of the epistemic
118 uncertainty related to source modeling. Although there are many analyzed inverted slip models, e.g.
119 a comprehensive summary of estimated static stress drops for the 2011 Tohoku earthquake by
120 Brown et al. (2015), major 11 inverted models (Ammon et al., 2011; Fujii et al., 2011; Hayes, 2011;

121 Iinuma et al., 2011, 2012; Shao et al., 2011; Yamazaki et al., 2011; Gusman et al., 2012; Satake et
122 al., 2013) are considered for defining the parameterization for the stochastic earthquake slip
123 distributions. The adopted inversion models have different fault dimensions as well as asperity
124 characteristics. Therefore, a wide range of admissible tsunami scenarios for an M_w9 mega-thrust
125 subduction earthquake in the Tohoku region can be explored, facilitating a detailed sensitivity and
126 variability analysis. For each model, source variations with stochastic slip realizations are
127 synthesized (50 cases per model; thus in total, 550 cases for the 11 inversion models). Note that the
128 stochastic source models generated in this study are intended to cover a wide range of possible
129 earthquake scenarios that may be applicable to probabilistic tsunami hazard mapping. Because the
130 stochastic source models are parameterized by spectral characteristics of a given source model, we
131 examine how different reference inversion models change probabilistic tsunami height and
132 inundation through the stochastic source modeling. Moreover, our investigations produce high-
133 resolution tsunami hazard information with 50-m grid resolution (compared to 450-m grid
134 resolution in Goda et al. [2014]). Tsunami hazard parameters considered are (i) the spatial
135 inundation depth and (ii) the inundated area where depth exceeds certain thresholds. We then
136 quantify the variations of these tsunami hazard estimates due to variability in slip distribution and
137 inversion-based source models. The results of this study are particularly useful for evaluating the
138 range of tsunami predictions for a broadly defined scenario, and relate specific inundation scenarios
139 to specific tsunami source characteristics for tsunami risk management.

140 This study is organized as follows. Section 2 summarizes stochastic source models used in the
141 tsunami simulation, including 11 published slip models for the 2011 Tohoku earthquake. Our
142 tsunami simulation set-up is described in Section 3. Section 4 presents tsunami simulations using
143 different earthquake slip models. The study focuses on ten major communities, located at the
144 Pacific side of the Tohoku region, to carry out tsunami impact assessments. In Section 5, tsunami
145 scenarios that produce critical hazard impacts are investigated in more detail to identify the most

146 critical scenarios for tsunami hazard mapping purposes. Finally, Section 6 summarizes the main
147 conclusions of this study.
148
149 ## 2 Stochastic earthquake source modeling using multiple inversions
150 This study considers multiple earthquake sources for synthetic rupture model generation to
151 examine the sensitivity of tsunami inundation characteristics to earthquake properties. First, we
152 provide an overview of earthquake source inversion results for the 2011 Tohoku earthquake and
153 resulting seafloor displacements. Next, we briefly review the method of stochastic earthquake
154 source simulation (Goda et al., 2014), followed by the tsunami source generation results that use the
155 described source modeling approach.
156
157 ### 2.1 *Inversion models of the Tohoku 2011 Earthquake Tsunami*
158 Multiple earthquake slip models are gathered from published source inversion studies for the
159 2011 Tohoku earthquake. These models are used as reference to further synthesize stochastic slip
160 distributions that resemble key features of the reference models (e.g. slip distribution and its
161 spectral characteristics in the wavenumber domain; see Section 2.2).
162 Table 1 summarizes key features of 11 rupture models deployed in this study, the
163 corresponding slip distributions are shown in Fig. 1. These source models are inverted using
164 teleseismic/tsunami/geodetic data to constrain fault displacement (slip) across the rupture plane.
165 Moment magnitudes of the source models range between 9.0 and 9.2, which translates into a factor
166 of two difference in seismic moment (or a factor of two in mean slip in case of identical fault
167 dimensions). Notable differences in slip models are observed in terms of fault plane dimensions, as
168 well as location and concentration of large slip patches (i.e. asperities). The fault length varies from
169 340 km (model 6) to 625 km (model 9), while the fault width ranges from 200 km to 260 km. The
170 depth to the top-edge of the fault plane varies from 0 km (models 1 and 2) to 7.4 km (models 4 and
171 5), while the fault strike falls between 192º to 202º, approximately parallel to the Japan Trench.

172 Models 1, 3 to 7, and 9 assume constant dip (between 10º and 14º), whereas other models have
173 variable dip angles that gradually steepen with increasing depth. The rake angles vary slightly,
174 representing reverse fault mechanisms (near 90º).

175 The characteristics of slip asperities, such as location, size, shape, and amplitude, differ
176 significantly among these source models, reflecting the complexity and uncertainty in imaging the
177 earthquake rupture process. In Fig. 1, regions outlined by thick black lines represent the asperity
178 area, defined as the regions in which slip is equal to or greater than three times the overall average
179 slip. Models 2, 6, and 11 have large asperities along the eastern edge of the fault plane, while others
180 have large slip values near the hypocenter. The maximum slip values for the 11 models reach 35 m
181 to 75 m. Models 3, 5, and 7 are characterized by slip concentration extending primarily along strike,
182 whereas models 1, 4, and 8 have circular/elliptic slip concentration. Other important features of the
183 models are different spatial resolutions of the inverted slip distributions, which affect the spectral
184 analysis and synthesis of stochastic slip models (Mai and Beroza, 2002; Goda et al., 2014).

185 Differences in earthquake slip result in different boundary conditions for the tsunami
186 excitation and propagation, and therefore also for the resulting run-up. Typically, the vertical
187 seafloor displacement is directly taken as the initial water surface elevation, evaluated based on
188 expressions of Okada (1985) and Tanioka and Satake (1996). The latter equation accounts for the
189 effects of horizontal seafloor movements in case of significant seafloor topography, which induces
190 additional vertical water-column motion. This approach is depicted in Fig. 2, showing vertical
191 seafloor displacements for the 11 inversion models. Clearly, variable slip patterns among source
192 models, even for the same event, generate very different spatial characteristics of seafloor
193 displacements, which in turn lead to different tsunami wave profiles at various locations along the
194 Tohoku coast (Goda et al., 2014).

195

196 ## 2.2 *Spectral analysis and synthesis of earthquake slip models*

The earthquake slip modeling procedure deployed in this study generates earthquake slip distributions based on spectral analysis of an inversion-based source model (hereafter, original slip model), resulting in simulated slip distributions that are statistically equivalent to the original slip model. The synthetic method is based on Mai and Beroza (2002), and has been recently modified for large mega-thrust subduction earthquakes (Goda et al., 2014). The random-field generation method is designed to balance similarity in key features of the inversion-based models (e.g. overall slip distribution and its spectral characteristics) with dissimilarity in the details (e.g. locations of large slip patches). A graphical flowchart of the procedure is shown in Fig. 3, using the Satake et al. (2013) slip distribution as an example (see the Spectral Analysis and Synthesis panel). The procedure begins with a spectral analysis of the reference source models (inversion results), based on which stochastic synthetic slip models are generated. Subsequently, these are used to carry out tsunami simulations for the targeted region, for which then a sensitivity analysis examines the relations between rupture properties and inundation characteristics. In the following, we describe these steps in more detail.

STEP1: Box–Cox analysis

Slip values of an inversion-based rupture model may be significantly different from the normal distribution and exhibit a heavy right-tail, in comparison with the normal distribution with the same statistics (Thingbaijam and Mai, 2016). To deal with non-normal slip distribution, a nonlinear scaling of slip values is considered during the random-field generation procedure (see STEP3). To identify a suitable nonlinear scaling method, the characteristics of the slip distribution are analyzed using the Box–Cox transformation (Box and Cox, 1964), in which an original variable x (i.e. non-normal slip values) is converted into y as: $y = (x^{\lambda}-1)/\lambda$. The method identifies the best power transformation parameter λ by maximizing the linear correlation coefficient between the transformed variable y and the standard normal variate for different values of λ. The obtained value

of λ is then used for nonlinear scaling of the synthesized slip distributions in spectral synthesis later (i.e. inverse Box–Cox transformation).

STEP2: Spectral analysis

Prior to the spectral analysis, the original slip model is bilinearly interpolated in space and then tapered to decrease slip to zero at each side of the fault plane (see sensitivity of tapering in Goda et al., 2016), which was considered to deal with different slip models. Subsequently, the fast Fourier transform (FFT) is applied to the interpolated slip distribution to obtain the two-dimensional (2D) normalized power spectrum. The usable wavenumber range ($k_{min} < k < k_{max}$) is determined based on the characteristic dimension of the fault plane (k_{min}) and the spatial resolution of the original slip model (k_{max}). The extracted normalized power spectra in the down-dip and along-strike directions are fitted by the power spectrum of an auto-correlation function. The power spectrum $P(k)$ of an anisotropic von Kármán auto-correlation function is considered:

$$P(k) \propto \frac{A_x A_z}{(1+k^2)^{H+1}}, \tag{1}$$

where k is the wavenumber, $k = (A_z^2 k_z^2 + A_x^2 k_x^2)^{0.5}$, A_z and A_x are the correlation lengths for the down-dip and along-strike directions, respectively, and H is the Hurst number. The value of H determines the slope of the power spectral decay in the high wavenumber range (Mai and Beroza, 2002). At wavenumber scales greater than the correlation length, the slip distribution is governed by average slip, while at wavenumber scales less than the correlation length, local slip heterogeneity dominates. A_x and A_z control the absolute level of the power spectrum in the low wavenumber range (i.e. $k << 1$) and differences in A_x and A_z capture anisotropic features of the slip distribution. H determines the power-spectral decay in the high wavenumber range, and theoretically is constrained to the range $0 \leq H \leq 1$, where smaller H implies rougher slip. The characteristic spectral values are different in the source models and depend on inversion methods even for the same event.

STEP3: Synthetic slip generation

Using the results from STEP2, multiple realizations of slip distributions are generated, applying the desired stochastic properties and the macroscopic source and spectral parameters. A random field, having quasi-normal distribution with a desired spatial correlation structure, is synthesized using a Fourier integral method (Pardo-Iguzquiza and Chica-Olmo, 1993). The amplitude spectrum of the target slip distribution is specified by the theoretical von Kármán power spectrum with correlation lengths and Hurst number estimated in STEP2, while the phase spectrum is represented by a random phase. The constructed complex Fourier coefficients are transformed into the spatial domain via 2D inverse FFT. The synthesized slip distribution is then nonlinearly scaled using the Box–Cox parameter λ estimated in STEP1 in order to follow the observed right-tail characteristics. In this re-scaling procedure, an upper bound (i.e. maximum slip of the original inversion model) is applied to avoid unrealistically large slip.

To ensure that the synthesized slip distributions resemble the original one in terms of location and amplitude of high-slip patches, their asperity dimensions are qualitatively compared with the original slip distribution. An acceptable slip distribution is required to have its maximum slip patch within the asperity zone of the original distribution, with its slip concentration located in the rectangular asperity zone greater than the threshold value given by the original slip distribution (see an example of spectral synthesis of the distribution in the right upper panel in Figure 3). This procedure constrains the spatial concentration of synthetic slip along the strike and dip. To implement this consistency check, multiple realizations are generated and compared against the original slip model. Finally, the mean and standard deviation of the transformed slip distribution are adjusted to adapt the statistics of the synthesized slip model to the original slip model.

To create the stochastic slip distributions for each of the 11 inversion models, 50 realizations of a target slip distribution are generated, with geometrical parameters identical to those of the original inversion models. Therefore, we perform the tsunami sensitivity and variability analyses for a total of 550 synthetic slip distributions. Table 2 lists the corresponding stochastic slip parameters for spectral synthesis. All Hurst numbers are set to 0.99, except for models 2 and 6, to constrain this

parameter within a physically meaningful range (i.e. $H < 1.0$). When $A_x > A_z$, the slip distribution is more coherent in along-strike direction, and thus slip appears anisotropic. The Box–Cox parameter λ captures the right-tail characteristics of slip distribution, with $\lambda = 0.0$ defining the logarithmic transformation and $\lambda = 1.0$ corresponding to the normal distribution. All Box–Cox parameters, except for model 11, are positive (between 0.1 and 0.3), indicating that the right-tail characteristics of these slip models are less heavy than the logarithmic case but heavier than the normal distribution. The heavy right-tail feature of model 11 ($\lambda = 0.0$) is attributed to very large slip values (exceeding 70 m) for several sub-faults along the trench (see Fig. 1). For approximately constant seismic moment, mean slip values of the original inversion models decrease with increasing fault dimensions. The fractional values for the size and the slip concentration of an asperity zone quantify asperity characteristics, and are subsequently used to determine acceptance/rejection of the synthesized slip distributions. Typically, 25% to 45% of the total slip is concentrated in only 9% to 13% of the overall rupture area (e.g. Mai et al., 2005). Therefore, the slip distributions simulated in this study exhibit by design macroscopic spectral slip characteristics that are statistically similar, but not identical, to the original inversion models.

3 Numerical tsunami modeling

Tsunami modeling is carried out using a well-tested numerical code (Goto et al. 1997) that computes the off-shore tsunami propagation and inundation profiles. The governing equations are the nonlinear shallow water equations, evaluated using a leap-frog staggered-grid finite difference scheme. The inundation calculation is performed by a moving boundary approach, where a dry or wet condition of a computational cell is determined based on total water depth. The computational domains are nested at four resolutions from offshore to onshore domains (i.e. 1350-m, 450-m, 150-m, and 50-m domains). Computational cells include those on land, and coastal defense structures are taken into account using overflowing formulae as a sub-grid model along the cell boundary as the most of urban areas in Japan is protected by coastal dikes.

Bathymetry/elevation data, Manning's roughness coefficients, and information of coastal defense structures for the Tohoku region are obtained from the Cabinet Office of the Japanese Government. The ocean bathymetry is based on the digital bathymetry data and nautical charts developed by the Japan Hydrographic Association and the Japan Coastal Guard. The land topography is based on the 50-m grid digital elevation model (DEM) developed by the Geospatial Information Authority of Japan. Note that the 50-m grid DEM data only represent an average value for a given cell, and hence yield rough approximations of land elevation at individual cells. The land use is considered to define bottom friction using Manning's formula, although subgrid scale strucutures are important to simulate local tsunami behavior (e.g. Liu et al., 2013). Four Manning's coefficients are assigned to computational cells based on national land use data in Japan: 0.02 $m^{-1/3}s$ for agricultural land, 0.025 $m^{-1/3}s$ for ocean/water, 0.03 $m^{-1/3}s$ for forest vegetation, and 0.04 $m^{-1/3}s$ for urban areas. Numerical tsunami calculations are performed for total event duration of 2 hours, using an integration time step of 0.5 s.

4. Sensitivity and variability of inundation areas along the Tohoku coast

4.1 *Outline of validation procedure*

The simulated inundation heights caused by the 11 original rupture models are compared against measured inundation and run-up observations from the 2011 Tohoku Tsunami Joint Survey (TTJS; Mori et al., 2011, 2012). The inundation heights in the TTJS database are converted to inundation depths using the 50-m grid DEM data from the Cabinet Office. Although such adjustments may be inaccurate for individual survey sites (e.g. at very steep hills), they are justified for the majority of flat terrains. To facilitate the comparison of spatial and depth extent of simulated inundation with the actual inundation/run-up observations, we consider ten strongly affected cities/towns along the Tohoku coast (Fraser et al., 2013). These are, from North to South (see Fig. 4): Miyako, Kamaishi, Ofunato, Rikuzentakata, Kesennuma, Onagawa, Ishinomaki–Higashimatsushima, Shiogama–Shichigahama, Sendai–Natori–Iwanuma, and Watari–Yamamoto–

Soma. Detailed results for three locations (Kamaishi, Onagawa, and Sendai–Natori–Iwanuma) are discussed in Sections 4.2, 4.3, and 4.4, respectively, whereas overall results for the ten locations are discussed in Section 4.5. These three locations are selected due to different positions with respect to the rupture plane and slip asperities (near for Onagawa, but far for the other locations) and steep fjord-like coast (Sanriku ria coast for Kamaishi and Onagawa) versus plain coast (Sendai coast for Sendai–Natori–Iwanuma), thus representing typical situations for the 2011 Tohoku tsunami.

For these post-surveyed sites, we compute various summary statistics of the simulated inundation depths and tsunami hazard parameters: mean and standard deviation of the inundation depths, inundation areas with depths exceeding threshold values of 1, 2, 3, 5, 7.5, and 10 m, and the K and κ factors (Aida, 1978). The K factor is the geometric mean of the ratio between the observed and simulated inundation/run-up heights, while the κ factor is the logarithmic standard deviation of the ratio. The corresponding equations are as follows:

$$\log_{10} K = \frac{1}{n}\sum_{i=1}^{n} \log_{10} H_{obs,i} / H_{simu,i} , \tag{2}$$

and,

$$\log_{10} \kappa = \sqrt{\frac{1}{n}\sum_{i=1}^{n} (\log_{10} H_{obs,i} / H_{simu,i})^2 - (\log_{10} K)^2} , \tag{3}$$

where n is the number of data points, and H_{obs} and H_{simu} are the observed and simulated inundation/run-up heights, respectively. The K factor becomes unity if the simulated inundation height is in perfect agreement with the observed inundation height, it decreases ($K < 1$) if the simulated inundation height is larger than the observation. To avoid undesired effects due to small values on the calculated performance metrics, inundation depths shallower than 0.5 m are excluded from the evaluation. Table 3 summarizes the mean and standard deviation of the simulated inundation depths at all ten locations for the 11 slip models; Table 4 lists the corresponding K and κ factors.

350 4.2 *Kamaishi in Iwate Prefecture*

351 Kamaishi is situated in an East-facing bay, with urban development concentrated along
352 Katsushi River. It is bounded by steep hills to the North and South. The port of Kamaishi was
353 protected by the deepest breakwaters in the world (foundation depth of 63 m, freeboard at 6 m
354 height above the sea surface), whose construction was completed in 2009. Although the Kamaishi
355 breakwaters were severely damaged during the 2011 Tohoku tsunami, the breakwaters were
356 effective in reducing the tsunami waves and delaying the arrival of major waves at the urban areas
357 of Kamaishi (Mori et al., 2013, 2015). Nonetheless, the tsunami damage and fatalities in Kamaishi
358 were devastating (Fraser et al., 2013). Based on the numerical analysis, the reduction of tsunami
359 height was estimated as 20-30 %, in comparison with similar locations near Kamaishi Bay with or
360 without breakwater (Mori et al., 2014). In the coastal defense data that are used for tsunami
361 simulation in this study, the Kamaishi breakwaters are represented partially; the northern section of
362 the Kamaishi breakwaters exists, whereas about 30% of the southern section of the Kamaishi
363 breakwaters is present in the coastal defense data followed by the field observations immediately
364 after the event.

365 Fig. 5 compares simulated inundation depth contours in Kamaishi for the 11 slip models,
366 including the TTJS results (color-coded circles). Comparing the inundation depth contours reveals
367 that the inundation area is not greatly affected by the slip model. In contrast, the water depths along
368 the shoreline and in low-lying areas are significantly different for the considered slip models,
369 because Kamaishi is surrounded by steep hills that prevent further inundation. Examining the
370 inundation contours, the source models can be categorized into two groups; models 1, 2, 7, 8, and 9
371 produce moderate inundation depths, whereas the remaining models (3, 4, 5, 6, 10, and 11) generate
372 extensive inundation depths (see Table 3). The simulation results for group 1 are in closer
373 agreement with the TTJS data than group 2. This is consistent with values of the K factor for group
374 1 (ranging between 0.68 and 0.90; Table 4), which indicate only moderate over-prediction.

375 Fig. 6 shows probability distributions for inundation areas for the city of Kamaishi due to
376 stochastic slip variations, using depth thresholds of 1 m and 5 m. The probability distributions are
377 derived for the 11 reference models individually to examine the effects of the reference source
378 model on the inundation characteristics. For a given reference model, a higher threshold value for
379 inundation areas (i.e. 5m versus 1m), shifts the probability distribution curve to the left, because
380 inundation areas with deeper depths are smaller than those with shallower depths. Note that the
381 local topography in Kamaishi affects the probability distribution of inundation areas for the
382 different slip models in various ways, depending also on the chosen depth threshold. When the
383 depth threshold of 1 m is considered (Fig. 6a), the inundation areas for all 11 models are bounded at
384 around 2.5 km^2, exhibiting greater consistency among different source models. On the other hand,
385 for the 5 m threshold (Fig. 6b), the probability distributions for the 11 models are more scattered.
386 This suggests that using one particular reference model for generating stochastic slip distributions
387 may not produce a robust inundation estimate. Thus, it is essential to consider alternative slip
388 scenarios in exploring the possible range of tsunami inundation footprints.

389 Fig. 7 shows the K and κ factors (Eqs. 2 and 3) for the stochastic slip distributions. The K
390 factor distributions for the 11 models show a wide range from 0.3 to 3.0 (especially at higher
391 probability levels), whereas the κ factor is more stable with respect to the alternative slip models. It
392 is interesting to point out that the probability levels corresponding to the K factor of 1.0 strongly
393 depend on the source models (ranging from 0.35 to 0.85), indicating that a retrospective association
394 of the 2011 Tohoku tsunami (i.e. benchmark historical event) with future tsunami hazard estimates
395 depends on the selected source model.

396

397 4.3 *Onagawa in Miyagi Prefecture*

398 Onagawa is situated in a narrow valley exposed to the ocean in the East. Because of its
399 location and topography, very large tsunami waves were generated by the 2011 Tohoku earthquake.
400 In particular, the majority of buildings in low-lying areas were completely inundated and destroyed;

401 the maximum inundation depths exceeded 16 m. In addition to the direct tsunami effects, a large
402 subsidence of 1.2 m was observed in Onagawa due to coseismic deformation of the 2011 Tohoku
403 earthquake. Because of the very large tsunami waves arriving within a relatively short time after the
404 earthquake (about 30 minutes), the fatality rate among the population residing in the inundated
405 areas was particularly high in Onagawa (Fraser et al., 2013).

406 The spatial distributions of inundation depth in Onagawa, located close to the epicenter and
407 major asperities, for the 11 original models are compared in Fig. 8. The areal coverage of
408 inundation is similar for the 11 models but with varying depths. Among the 11 models, models 4, 5,
409 and 7 produce particularly extensive inundation depths in Onagawa's low-lying areas (Table 3). The
410 results based on models 2 and 6 are consistent with the TTJS data (Table 4). The large differences
411 between the estimated inundation extent in Onagawa are related to the major asperities off the
412 northern Miyagi ria coast; these high-slip regions are located relatively deep on the fault, rather than
413 at shallow depths along the trench (Fig. 1). The latter observation is in agreement with Satake et al.
414 (2013) who investigated the effects due to deep versus shallow slips on tsunami waves.

415 The plots of the probability distribution functions for different source models (Fig. 9) reveal
416 limited sensitivity to the source models, compared to other locations in ria regions, i.e. the coastal
417 line formed by submerged river valleys (see Fig. 6 for Kamaishi). The cumulative probability
418 distribution functions for the different source models have similar profiles but different starting
419 values of inundation area because all source models contain large slip patches off northern Miyagi
420 Prefecture (Fig. 1), while the inundation areas are practically bounded at 1 km^2 due to topographic
421 features of Onagawa.

422 Fig. 10 shows the variability of the K and κ factors due to the slip variations. The K factor
423 distributions reveal remarkable differences among the 11 slip models, ranging from 0.3 to 5.0,
424 although their overall trends are similar to Kamaishi (Fig. 7). One group of reference models
425 (models 4 to 8) shows a steep probability increase for the K factor less than 1.0 (i.e. the majority of
426 the stochastic slip distributions produce tsunami inundation extent similar to or greater than the

observed inundation during the 2011 Tohoku tsunami). In contrast, other models show particularly wide variations. The former group tends to have major asperities off northern Miyagi Prefecture, whereas the latter group allows shifts of major asperities toward the North and South of Onagawa. The slip models giving larger *K* factors in Onagawa (models 2, 3, and 9 to 11) act differently for Kamaishi (models 1, 2, 7, 9, and 10), although the slip models giving smaller *K* factors are similar at the two locations. Because the upper extent of inundation in ria coastal regions is limited by the surrounding steep hills that act as barriers for extreme inundation, the *K* factor is restricted at the lower limits (Figs. 7 and 10). Since the probability levels corresponding to $K = 1.0$ vary between 0.15 and 0.8, it is difficult to claim that the 2011 Tohoku event was a rare case for Onagawa, compared to the stochastic scenarios based on a few reference models. Therefore, multiple reference models are required to comprehensively characterize the potential tsunami hazard in this region.

4.4 *Sendai–Natori–Iwanuma in Miyagi Prefecture*

Sendai, Natori, and Iwanuma are positioned in the Sendai plain (Figure 4), and represent the most densely populated areas in Miyagi Prefecture. Two major rivers, the Natori River and Abukuma River, run through these regions. The flat terrain contributed significantly to the wide-spread inundation during the 2011 Tohoku tsunami that even reached the Sendai Tobu Highway that runs South-North at about 2 to 5 km from the coast. The 10-m embankment of the highway reduced the tsunami inundation significantly (Goto et al., 2012). The destruction of residential districts near the shoreline (e.g. Arahama and Yuriage) was particularly severe. Because of the unexpectedly large tsunami, the fatality rates in the severely inundated areas were relatively high (Fraser et al., 2013).

The inundation depth in Sendai–Natori–Iwanuma, shown in Fig. 11, strongly depends on the source model, which is different than for other ria coast regions (Figs. 7 and 8). For the 11 slip models, the spatial extent of inundation is only moderately affected by the source models, but the

depth extent along the shoreline varies greatly. Models 4, 5, 7, and 11 over-predict the observed inundation depths, while model 9 under-predicts the observations (Table 3). Although the effects of the embankment at the Sendai Tobu Highway (Goto et al., 2012) are not taken into account in the tsunami simulations due to model resolution, the results based on models 2, 6, and 8 are consistent with the observations (Table 4). As Sendai, Natori, and Iwanuma are on a flat terrain, inundation depth as well as its spatial extent are critically important for tsunami hazard assessment.

The sensitivity analysis for inundation areas for depth thresholds of 1 m and 5 m suggests that large variability of inundation extent for the 11 reference models can also be observed from the wide probability range covered in Fig. 12a, indicating that the slip distributions from the 11 models can be separated into two groups in terms of their behavior in the probability distribution functions. In case of the 1 m threshold (Fig. 12a), models 9 to 11 show a gradual and constant increase of the probability distribution, while all other slip models generate extensive inundation scenarios for the majority of the cases (e.g. steep increase of the curves around 100 km^2). An explanation for this broad range of inundation areas for models 9 to 11 is the smaller slip amount in the southern part of the Tohoku region (model 9) in comparison with other models, while the majority of large slip patches faces the Tohoku ria region, rather than the Sendai coastal region (models 10 and 11). Similar tendencies for separation into two groups are observed for other parts of the Sendai coastal plain (e.g. Ishinomaki–Higashimatsushima and Shiogama–Shichigahama). The overall inundation areas are limited due to topographical constraints, although it is quite large in the Sendai plain (e.g. 140 km^2 in Sendai–Natori–Iwanuma).

The variability of the K and κ factors due to stochastic slip distributions is shown in Fig. 13. Separation into two distinct groups for the K-factor suggests that it is imperative to consider a range of alternative reference models when generating stochastic slip distributions for tsunami hazard analyses. Interestingly, the κ factor for the 11 models is essentially identical.

4.5 *Combined results for ten cities and towns in the Tohoku region*

479 The sensitivity and variability of inundation areas with respect to variations in earthquake
480 source characteristics are integrated by considering all ten selected locations. The results for the
481 combined areas are similar to those for coastal plain regions. For instance, two distinct groups can
482 be identified in the probability distributions for the slip variations. This is expected because the
483 adopted metrics are the total inundation areas at the ten locations along the Tohoku coast. The same
484 observations can be obtained from the K and κ factor plots. According to the K factors calculated
485 for the combined areas (Table 4), models 2 and 8 perform well overall in reproducing the observed
486 inundation depths during the Tohoku tsunami, followed by models 1 and 6. This observation could
487 have been anticipated, since models 1, 2, 6, and 8 are estimated by tsunami inversion, while the
488 others are based on different data sets (Table 1). However, the sensitivity and variability of the
489 inundation characteristics at different locations do not show comparable (consistent) behavior, but
490 instead reveal location-dependent trends. Therefore, the local inundation characteristics can be
491 significantly different for the various cases, depending on fault geometry, relative location to
492 epicenter and local bathymetry-topography effects.
493
494 **5 Critical scenarios for tsunami hazard mapping**
495 Stochastic earthquake slip scenarios generated by spectral analysis and synthesis of inverted
496 source models are useful to investigate the sensitivity of tsunami properties to slip distribution and
497 vertical seafloor displacement. Therefore, they help to define critical hazard thresholds and potential
498 consequences. Assuming that a set of generated earthquake slip distributions constitutes a suitable
499 representation for computing possible future tsunami scenarios, one can examine the relationships
500 between inundation extent at a particular location/region and slip distribution/vertical seafloor
501 displacement at different hazard levels (based on all admissible slip distributions for a given
502 earthquake scenario). This essentially closes a loop in tsunami hazard analysis by more rigorously
503 quantifying the uncertainty associated with tsunami predictions, allowing also identifying the most

important parameters that drive the tsunami hazard. This is conceptually similar to tsunami hazard disaggregation (Geist and Parsons, 2006; Thio et al., 2007; Horspool et al., 2014).

In this study, a set of 550 stochastically generated slip realization based on the 11 slip models is adopted as a representative set. Although further refinement of these slip models (or their selection) may be considered by utilizing expert opinions or physics-based algorithmic selection criteria, the results demonstrate highly complicated inter-dependency of inundation properties due to site condition, site location, and earthquake source properties.

To investigate critical scenarios for tsunami hazard and risk reduction, three particular locations, Kamaishi, Onagawa, and Sendai–Natori–Iwanuma, are examined in detail. For each location, 550 slip models are sorted in an ascending order according to an adopted tsunami hazard metric. For illustration, the inundation areas above 1 m depth are considered. Then, a slip model that corresponds to the 10th-, 50th-, or 90th-percentile in terms of the adopted metric is identified (these percentiles may represent the least, a typical, and the worst case scenario, respectively). Figs. 14 to 16 show three sets of slip distributions and vertical seafloor displacements, identified based on the above-mentioned procedure for Kamaishi, Onagawa, and Sendai–Natori–Iwanuma. Note that the shown slip seafloor displacement represents just one of the possible scenarios that lead to the specified hazard levels. In each figure, the inundation areas above 1 m depth are indicated, corresponding to the 10th-, 50th-, and 90th-percentile levels and reference source models (see Table 1 and Fig. 1). Although the three percentile levels are distributed evenly with respect to the median, the inundation areas corresponding to these percentile levels are unevenly distributed because inundation processes are highly nonlinear (Figs. 5 to13).

Fig. 14 shows that the 10th-percentile scenario does not have major slip patches off-shore Kamaishi (marked as a circle with grey-color fill). Therefore, the tsunami waves do not affect Kamaishi directly. If a higher percentile level is considered, locations of major slip patches move North, leading to more extensive tsunami inundation for such scenarios. Note that the inundation areas above 1 m depth for the 90th-percentile scenario are greater by a factor of 2.5 than those for

530 the 10th-percentile scenario. Figs. 15 and 16 show the critical slip distributions and vertical seafloor
531 displacements for Onagawa and Sendai–Natori–Iwanuma. The general observations for Kamaishi
532 are also applicable to these locations: with an increase of percentile level, slip patches move closer
533 to the region. The relative changes of the inundation areas from one percentile level to another
534 depend on the location.

535 Finally, the results for the combined areas of 10 cities and towns are also evaluated, but not
536 presented in detail since they are very similar to those for Sendai–Natori–Iwanuma (i.e. Fig. 16).
537 The results indicate that for the 10th-percentile case, large slips exist off the Sanriku coast. In these
538 cases, the total inundation areas are smaller but major tsunami waves will still hit communities in
539 the ria regions (potentially causing catastrophic damage). At the 50th-percentile level, the slip
540 concentrations move South, causing more extensive inundation in coastal plain regions. For the
541 90th-percentile case, the asperities move even further South and increase in size. For a particular
542 target location, the worst-case scenario is given in case of nearby high-slip region. Therefore, the
543 estimation of the maximum slip and its possible location (e.g. along the trench) is important to
544 improve stochastic tsunami hazard assessments.

545 As a final remark, it is important to recognize that critical scenarios at different hazard levels
546 correspond to different slip characteristics, and do not occur simultaneously. Therefore, different
547 scenarios are useful for different regions and different purposes. For example, local municipalities
548 may be interested in preparing a set of tsunami hazard maps for evacuation purposes, and thus
549 stochastic tsunami scenarios and corresponding inundation maps for local communities are useful.
550 On the other hand, from a wider regional perspective, emergency managers should prepare several
551 tsunami scenarios and corresponding inundation maps for the region in order to assess the tsunami
552 hazard at different locations for a range of critical scenarios. Although it is not straightforward to
553 decide how to utilize and communicate such comprehensive statistical tsunami hazard information,
554 (as presented in this study) to the general audience and decision makers, it is important to
555 understand the range of uncertainty in terms of tsunami consequences for a given scenario. To

556 successfully implement tsunami risk mitigation, results of probabilistic tsunami hazard assessments
557 need to be properly summarized and presented to residents and policy makers.
558
559 **6 Conclusions**
560 Tsunami inundation is a highly nonlinear process that is strongly influenced by tsunami-
561 generation due to earthquake source characteristics and by the local topography. In this study, we
562 developed and applied a new framework for assessing the sensitivity and variability of tsunami
563 inundation due to a mega-thrust subduction earthquake. We then quantified the sensitivity and
564 variability of tsunami hazard parameters (inundation depths, inundation areas with different depth
565 thresholds, and K and κ performance metrics) at various locations along the coast for multiple
566 reference earthquake source models and their stochastic realizations. The assessment of the
567 sensitivity and variability of the tsunami hazard parameters facilitates the broader exploration of
568 possible tsunami scenarios and their potential consequences. It also provides tsunami analysts and
569 local stakeholders with important information for improved tsunami risk management and
570 communication.
571 The main conclusions of this study are:
572 • The influence of the reference source models on the inundation sensitivity and variability is
573 significant, indicating that relying on one particular inversion model, as a representative case,
574 may lead to under-estimation of the total tsunami hazard and potential consequences. A
575 careful and scientifically justifiable selection of the reference model should be an essential
576 part of any such assessment, and a transparent method for selecting a set of applicable
577 reference source models needs to be developed. We recommended to use several available
578 source models as "representative" cases, also for calibration purposes, to generate a
579 sufficiently large set of different scenarios.
580 • The development of critical scenarios for tsunami hazard and risk assessments is important,
581 and closes the loop between variability assessment associated with tsunami predictions and

identification of high-impact scenarios for tsunami hazard mapping and disaster preparedness planning. The performance metrics should be selected carefully (e.g. inundation areas above different depth thresholds and *K* factor) and the context of the assessments (e.g. local versus regional) should be defined clearly to make critical scenarios meaningful for tsunami risk mitigation, because some aspects of the hazard characteristics may be masked unintentionally.

Acknowledgements

The bathymetry and elevation data for the Tohoku region were provided by the Cabinet Office of the Japanese Government. The run-up and inundation survey data were obtained from the 2011 Tohoku Earthquake Tsunami Joint Survey Group (http://www.coastal.jp/tsunami2011/). This work was supported by the Engineering and Physical Sciences Research Council (EP/M001067/1) as well as by the King Abdullah University of Science and Technology (KAUST; Research grant BAS 1339-01-01), and the Disaster Prevention Research Institute at Kyoto University.

References

Aida, I., 1978. Reliability of tsunami source model derived from fault parameters. J. Phys. Earth 26, 57–73.

Ammon, C.J., Lay, T., Kanamori, H., Cleveland, M., 2011. A rupture model of the 2011 off the Pacific coast of Tohoku earthquake. Earth Planets Space, 63, 693–696.

Box, G. E., Cox, D. R., 1964. An analysis of transformations. Journal of the Royal Statistical Society. Series B (Methodological), 211-252.

Brown, L., Wang, K., Sun, T., 2015, Static stress drop in the Mw 9 Tohoku-oki earthquake: Heterogeneous distribution and low average value. Geophysical Research Letters. 42, 10,595–10,600, doi:10.1002/2015GL066361.

606 Burbidge, D., Mueller, C., Power, W., 2015. The effect of uncertainty in earthquake fault
607 parameters on the maximum wave height from a tsunami propagation model. Natural Hazards
608 and Earth System Sciences, 15, 2299-2312.
609 Chock, G., 2016. Design for tsunami loads and effects in the ASCE 7-16 standard. Journal of
610 Structural Engineering, 142, 10.1061/(ASCE)ST.1943-541X.0001565 , 04016093.
611 Fraser, S., Pomonis, A., Raby, A., Goda, K., Chian, S.C., Macabuag, J., Offord, M., Saito, K.,
612 Sammonds, P., 2013. Tsunami damage to coastal defences and buildings in the March 11th
613 2011 M_w9.0 Great East Japan earthquake and tsunami. Bulletin of Earthquake Engineering, 11,
614 205–239.
615 Fujii, Y., Satake, K., Sakai, S., Shinohara, S., Kanazawa, T., 2011. Tsunami source of the 2011 off
616 the Pacific coast of Tohoku earthquake. Earth Planets Space, 63, 815–820.
617 Fukutani, Y., Suppasri, A., Imamura F. 2015. Stochastic analysis and uncertainty assessment of
618 tsunami wave height using a random source parameter model that targets a Tohoku-type
619 earthquake fault. Stochastic Environmental Research and Risk Assessment, 29, 1763–1779.
620 Geist, E.L., 2002. Complex earthquake rupture and local tsunamis. Journal of Geophysical Research,
621 doi:10.1029/2000JB000139.
622 Geist, E.L., Parsons, T., 2006. Probabilistic analysis of tsunami hazards. Natural Hazard, 37, 277–
623 314.
624 Goda, K., Mai, P.M., Yasuda, T., Mori, N., 2014. Sensitivity of tsunami wave profiles and
625 inundation simulations to earthquake slip and fault geometry for the 2011 Tohoku earthquake.
626 Earth Planets Space. 66, 105, doi:10.1186/1880-5981-66-105.
627 Goda, K., T. Yasuda, N. Mori and P.M. Mai, 2015a. Variability of tsunami inundation footprints
628 considering stochastic scenarios based on a single rupture model: application to the 2011
629 Tohoku earthquake. Journal of Geophysical Research Ocean, 120, 4552–4575.

630 Goda, K., S. Li, N. Mori and T. Yasuda, 2015b. Probabilistic tsunami damage assessment
631 considering stochastic source models: application to the 2011 Tohoku Earthquake. Coastal
632 Engineering Journal, 57, 1550015.
633 Goda, K., T. Yasuda, N. Mori and T. Maruyama, 2016. New scaling relationships of earthquake
634 source parameters for stochastic tsunami simulation, Coastal Engineering Journal. 58,
635 1650010.
636 Goto, C., Ogawa, Y., Shuto, N., Imamura, F., 1997. Numerical method of tsunami simulation with
637 the leap-frog scheme (IUGG/IOC Time Project). IOC Manual, UNESCO, No. 35, Paris,
638 France.
639 Goto, K., Fujima, K., Sugawara, D., Fujino, S., Imai, K., Tsudaka, R., Abe, T., Haraguchi, T., 2012.
640 Field measurements and numerical modeling for the run-up heights and inundation distances
641 of the 2011 Tohoku-oki tsunami at Sendai Plain, Japan. Earth Planets Space, 64, 1247–1257.
642 Gusman, A.R., Tanioka, Y., Sakai, S., Tsushima, H., 2012. Source model of the great 2011 Tohoku
643 earthquake estimated from tsunami waveforms and crustal deformation data. Earth Planet
644 Science Letters, 341–344, 234–242.
645 Hayes, G.P., 2011. Rapid source characterization of the 2011 Mw 9.0 off the Pacific coast of
646 Tohoku earthquake. Earth Planets Space, 63, 529–634.
647 Horspool, N., Pranantyo, I., Griffin, J., Latief, H., Natawidjaja, D.H., Kongko, W., Cipta, A.,
648 Bustaman, B., Anugrah, S.D., Thio, H.K., 2014. A probabilistic tsunami hazard assessment
649 for Indonesia. Natural Hazards and Earth System Sciences, 14, 3105–3122.
650 Iinuma, T., Ohzono, M., Ohta, Y., Miura, S., 2011. Coseismic slip distribution of the 2011 off the
651 Pacific coast of Tohoku earthquake (M9.0) estimated based on GPS data – was the asperity in
652 Miyagi-oki ruptured? Earth Planets Space. 63, 643–648.
653 Iinuma, T., Hino, R., Kido, M., Inazu, D., Osada, Y., Ito, Y., Ohzono, M., Tsushima, H., Suzuki, S.,
654 Fujimoto, H., Miura, S., 2012. Coseismic slip distribution of the 2011 off the Pacific coast of

655 Tohoku earthquake (M9.0) refined by means of seafloor geodetic data. Journal of
656 Geophysical Research, doi:10.1029/2012JB009186.
657 Kaiser, G., Scheele, L., Kortenhaus, A., Løvholt, F., Römer, H., Leschka, S., 2011. The influence of
658 land cover roughness on the results of high resolution tsunami inundation modeling. Natural
659 Hazards and Earth System Sciences. 11, 2521–2540.
660 Liu, H., Shimozono, T., Takagawa, T., Okayasu, A., Fritz, H.M., Sato, S. and Tajima, Y., 2013. The
661 11 March 2011 Tohoku Tsunami Survey in Rikuzentakata and Comparison with historical
662 Events. Pure and Applied Geophysics, 170(6-8), 1033-1046, doi:10.1007/s00024-012-0496-2.
663 Løvholt, F., Pedersen, G., Bazin, S., Kuhn, D., Bredesen, R.E., Harbitz, C., 2012. Stochastic
664 analysis of tsunami runup due to heterogeneous coseismic slip and dispersion. Journal of
665 Geophysical Research, doi:10.1029/2011JC007616.
666 MacInnes, B.T., Gusman, A.R., Le Veque, R.J., Tanioka, Y., 2013. Comparison of earthquake
667 source models for the 2011 Tohoku event using tsunami simulations and near-field
668 observations. Bulletin of the Seismological Society of America, 103, 1256–1274.
669 Mai, P.M., Beroza, G.C., 2002. A spatial random field model to characterize complexity in
670 earthquake slip. Journal of Geophysical Research Solid Earth. doi:10.1029/2001JB000588.
671 Mai, P.M., Spudich, P., Boatwright, J., 2005. Hypocenter locations in finite-source rupture models.
672 Bulletin of the Seismological Society of America, 95, 965–980.
673 Mai, P.M.,and K.K.S Thingbaijam (2014). SRCMOD: An online database of finite-fault rupture
674 model, Seismological Research Letters, Vol 85, 6, p. 1348-1357, doi: 10.1785/0220140077
675 McCloskey, J., Antonioli, A., Piatanesi, A., Sieh, K., Steacy, S., Nalbant, S., Cocco, M., Giunchi,
676 C., Huang, J.D., Dunlop, P., 2008. Tsunami threat in the Indian Ocean from a future
677 megathrust earthquake west of Sumatra. Earth Planet Science Letters, 265, 61–81.
678 Mori, N., Takahashi, T., Yasuda, T., Yanagisawa, H., 2011. Survey of 2011 Tohoku earthquake
679 tsunami inundation and run-up. Geophysical Research Letters, doi:10.1029/2011GL049210.

680 Mori, N., Takahashi, T., The 2011 Tohoku Earthquake Tsunami Joint Survey Group, 2012.
681 Nationwide post event survey and analysis of the 2011 Tohoku earthquake tsunami. Coastal
682 Engineering Journal, 54, 1250001-1-27.
683 Mori, N. Cox, D.T., Yasuda, T., Mase, H., 2013. Overview of the 2011 Tohoku earthquake tsunami
684 damage and its relation to coastal protection along the Sanriku coast. Earthquake Spectra. 29,
685 S127–S143.
686 Mori, N., Yoneyama, N., Pringle, W., 2015. Effects of the offshore barrier against the 2011 off the
687 Pacific coast of Tohoku earthquake tsunami and lessons learned. In: *Post tsunami hazards:*
688 *restoration and reconstruction* (V. Santiago-Fandino, Y.A. Kontar, Y. Kaneda, eds.),
689 Springer, pp. 121–132.
690 Mori, N., Goda K., Cox, D.T., 2017. Recent process in Probabilistic Tsunami Hazard Analysis
691 (PTHA) for mega thrust subduction earthquakes, In Reconstruction and Restoration after the
692 2011 Japan Earthquake and Tsunami: Insights and Assessment after 5 years, Springer, in
693 press.
694 Mueller, C., Power, W.L., Fraser, S., Wang, X. 2015. Effects of rupture complexity on local
695 tsunami inundation: implications for probabilistic tsunami hazard assessment by example.
696 Journal of Geophysical Research Solid Earth. **120**, doi:10.1002/2014JB011301.
697 Okada, Y., 1985. Surface deformation due to shear and tensile faults in a half-space. Bulletin of the
698 Seismological Society of America. 75, 1135–1154.
699 Pang, A., 2008. Visualizing uncertainty in natural hazards. Risk Gov. Soc. 14, 261–294.
700 Pardo-Iguzquiza, E., Chica-Olmo, M., 1993. The Fourier integral method: an efficient spectral
701 method for simulation of random fields. Mathematical Geosciences, 25, 177–217.
702 Park, Hyoungsu, and Daniel T. Cox., 2016. Probabilistic assessment of near-field tsunami hazards:
703 Inundation depth, velocity, momentum flux, arrival time, and duration applied to Seaside,
704 Oregon. Coastal Engineering. 117, 79-96.

Shao, G., Li, X., Ji, C., Maeda, T., 2011. Focal mechanism and slip history of the 2011 M_w 9.1 off the Pacific coast of Tohoku earthquake, constrained with teleseismic body and surface waves. Earth Planets Space. 63, 559–564.

Satake, K., Fujii, Y., Harada, T., Namegaya, Y., 2013. Time and space distribution of coseismic slip of the 2011 Tohoku earthquake as inferred from tsunami waveform data. Bulletin of the Seismological Society of America, 103, 1473–1492.

Tanioka, Y., Satake, K., 1996. Tsunami generation by horizontal displacement of ocean bottom. Geophysical Research Letters, 23, 861–864.

Thingbaijam, K.K.S., and P. M. Mai (2016). Evidence for truncated exponential probability distribution of earthquake, Bulletin of the Seismological Society of America, Vol. 106, No. 4, 1802-1816, doi: 10.1785/0120150291

Thio, H.K., Somerville, P., Ichinose, G., 2007. Probabilistic analysis of strong ground motion and tsunami hazards in southeast Asia. Journal of Earthquake and Tsunami, 1, 119-137.

Yamazaki, Y., Lay, T., Cheung, K.F., Yue, H., Kanamori, H., 2011. Modeling near-field tsunami observations to improve finite-fault slip models for the 11 March 2011 Tohoku earthquake. Geophysical Research Letters, doi:10.1029/2011GL049130.

721 Table 1. Summary of the 11 slip models.

Model ID and reference	Seismic moment (Nm)	Length (km)	Width (km)	Top-edge depth (km)	Strike, dip, rake (°)	Sub-fault number[1]	Sub-fault size[1] (km)	Data type
1: Fujii et al. (2011)	3.8×10^{22}	500	200	0.0	[193, 14, 81]	10×4	50×50	Tsunami
2: Satake et al. (2013)	4.2×10^{22}	550	200	0.0	[193, 8-16, 81]	11×5	50×50/25	Tsunami
3: Shao et al. (2011) [Ver1]	5.6×10^{22}	500	200	4.9	[198, 10, *Var*[2]]	20×10	25×20	Teleseismic
4: Shao et al. (2011) [Ver2]	5.8×10^{22}	475	200	7.4	[198, 10, *Var*]	19×10	25×20	Teleseismic
5: Shao et al. (2011) [Ver3]	5.8×10^{22}	475	200	7.4	[198, 10, *Var*]	19×10	25×20	Teleseismic
6: Yamazaki et al. (2011)	3.2×10^{22}	340	200	3.8	[192, 12, *Var*]	17×10	20×20	Teleseismic & tsunami
7: Ammon et al. (2011)	3.6×10^{22}	600	210	1.0	[202, 12, 85]	40×14	15×15	Teleseismic & geodetic
8: Gusman et al. (2012)	5.1×10^{22}	450	200	1.0	[202, 5-20, *Var*]	9×5	50×40	Tsunami & geodetic
9: Hayes (2011)	4.9×10^{22}	625	260	5.8	[194, 10, *Var*]	25×13	25×20	Teleseismic
10: Iinuma et al. (2011)	4.0×10^{22}	600	240	1.1	[*Var*, *Var*, *Var*]	60×24	10×10	Geodetic
11: Iinuma et al. (2012)	4.0×10^{22}	620	260	1.0	[*Var*, *Var*, *Var*]	62×26	10×10	Geodetic

722 1) The first entry is for the along-strike direction, while the second entry is for the down-dip direction, and 2) *Var* represents that the parameter is variable.

723 Table 2. Summary of the stochastic slip parameters for the 11 slip models.

Model ID	von Kármán parameters [A_z (km), A_x (km), H]	Grid spacing (km)	Box–Cox parameter	Mean and std. dev. of the original slip model[1] (m)	Asperity-zone dimension fraction[2] [down-dip, along-strike]	Asperity slip concentration fraction[3]
1	[63, 68, 0.99]	25	0.2	[7.18, 8.41]	[0.35, 0.35]	0.4
2	[56, 107, 0.82]	25	0.2	[9.43, 11.75]	[0.25, 0.4]	0.3
3	[50, 119, 0.99]	10	0.3	[11.85, 11.14]	[0.25, 0.4]	0.35
4	[53, 84, 0.99]	10	0.3	[10.71, 12.54]	[0.3, 0.4]	0.35
5	[45, 93, 0.99]	10	0.3	[11.14, 14.10]	[0.3, 0.4]	0.35
6	[37, 72, 0.96]	10	0.2	[14.20, 13.92]	[0.3, 0.4]	0.4
7	[51, 94, 0.99]	10	0.3	[7.84, 10.48]	[0.4, 0.35]	0.3
8	[64, 86, 0.99]	25	0.2	[9.38, 10.35]	[0.3, 0.35]	0.3
9	[65, 94, 0.99]	10	0.2	[5.27, 6.21]	[0.3, 0.4]	0.3
10	[54, 141, 0.99]	10	0.1	[8.32, 7.90]	[0.3, 0.3]	0.25
11	[51, 81, 0.99]	10	0.0	[7.95, 12.11]	[0.45, 0.3]	0.45

724 1) The slip model is the tapered original slip distribution; 2) The fraction values of the asperity rectangle for the
725 down-dip and along-strike directions are defined in terms fault length and fault width of the original slip model;
726 and 3) The fraction value of the asperity slip concentration is defined in terms of total slip over the fault plane.
727

728 Table 3. Mean and standard deviation of the simulated inundation depths for the 11 slip models.

City/town	TTJS	Model 1	Model 2	Model 3	Model 4	Model 5	Model 6	Model 7	Model 8	Model 9	Model 10	Model 11
Miyako	4.12, 2.65	3.11, 2.92	3.12, 2.71	3.37, 2.86	5.91, 3.16	7.82, 3.55	5.13, 3.35	2.50, 2.37	3.04, 2.58	2.00, 1.76	9.64, 3.72	10.28, 3.83
Kamaishi	5.42, 3.42	6.81, 2.58	6.91, 2.89	10.79, 2.84	10.51, 2.90	10.67, 2.90	10.29, 2.83	5.21, 2.64	5.81, 2.61	6.04, 2.69	13.83, 2.84	11.36, 2.72
Ofunato	7.69, 4.92	4.33, 2.71	4.93, 3.29	6.89, 4.43	6.43, 4.10	7.68, 5.95	6.25, 3.44	3.29, 2.18	3.49, 2.43	4.19, 2.96	4.66, 2.93	4.88, 3.15
Rikuzentakata	8.16, 4.58	8.16, 5.39	7.77, 5.19	9.22, 6.18	12.20, 5.99	8.47, 5.92	8.26, 5.42	8.29, 5.26	6.90, 4.77	5.81, 4.65	9.40, 5.87	9.13, 5.77
Kesennuma	4.35, 3.01	3.43, 2.34	2.88, 2.12	3.70, 2.55	4.18, 2.63	3.36, 2.65	4.24, 2.52	3.05, 2.18	2.69, 2.09	2.39, 2.03	2.69, 2.18	2.93, 2.44
Onagawa	7.74, 4.10	10.85, 5.06	7.37, 3.87	6.38, 3.61	18.89, 4.98	12.96, 4.97	6.74, 4.12	16.14, 4.99	5.83, 3.63	4.48, 3.59	10.26, 5.06	9.00, 4.00
Ishinomaki	2.49, 1.99	3.54, 2.02	3.20, 2.02	2.99, 2.16	5.25, 2.53	4.66, 2.25	2.92, 1.92	5.45, 2.27	2.17, 1.85	1.34, 1.52	2.84, 2.10	4.12, 2.37
Shiogama	3.58, 2.93	3.88, 3.07	3.65, 2.69	3.83, 3.43	5.41, 4.00	4.95, 3.65	3.77, 3.15	5.44, 3.46	3.17, 3.00	2.17, 2.60	3.31, 3.16	4.62, 3.71
Natori	2.71, 2.07	3.89, 1.59	3.28, 1.59	4.89, 1.88	6.30, 1.96	5.45, 1.93	3.70, 1.82	6.32, 1.49	2.83, 1.63	1.84, 1.53	4.05, 1.64	5.52, 1.99
Yamamoto	3.75, 2.79	3.70, 1.85	2.06, 1.51	5.43, 2.19	6.28, 2.15	5.93, 2.14	3.84, 2.06	7.43, 2.23	2.05, 1.58	1.08, 1.56	4.56, 2.13	5.76, 2.14

729

730 Table 4. *K* factor and κ factor of the simulated inundation depths for the 11 slip models. Cells having *K* factor between 0.9 and 1.1 are shaded
731 with grey color.

City/town	Model 1	Model 2	Model 3	Model 4	Model 5	Model 6	Model 7	Model 8	Model 9	Model 10	Model 11
Miyako	0.93, 1.79	1.05, 2.06	1.02, 1.98	0.64, 1.96	0.51, 1.96	0.78, 2.14	1.18, 1.88	1.15, 1.91	1.44, 1.66	0.38, 1.81	0.35, 1.83
Kamaishi	0.68, 1.81	0.71, 1.85	0.40, 1.78	0.42, 1.76	0.41, 1.77	0.43, 1.78	0.90, 1.59	0.84, 1.93	0.74, 1.63	0.31, 1.88	0.38, 1.79
Ofunato	1.72, 1.70	1.58, 1.72	1.15, 1.71	1.23, 1.68	1.06, 1.73	1.15, 1.57	2.33, 1.74	2.03, 1.69	1.82, 1.76	1.59, 1.79	1.55, 1.71
Rikuzentakata	0.98, 1.72	1.07, 1.75	0.94, 1.63	0.62, 1.56	1.03, 1.80	1.04, 1.59	0.97, 1.74	1.18, 1.80	1.53, 2.22	0.87, 1.50	0.95, 1.69
Kesennuma	1.26, 1.73	1.47, 1.78	1.16, 1.74	0.99, 1.69	1.31, 1.78	0.98, 1.64	1.44, 1.82	1.49, 1.74	1.75, 1.80	1.45, 1.69	1.40, 1.76
Onagawa	0.69, 1.74	0.98, 1.99	1.13, 2.01	0.34, 1.82	0.53, 1.67	1.03, 2.00	0.41 1.76	1.29, 2.08	1.68, 2.29	0.76, 1.76	0.77, 1.88
Ishinomaki	0.57, 1.91	0.64, 1.82	0.72, 1.95	0.38, 2.00	0.43, 1.96	0.71, 1.79	0.36, 1.98	1.05, 1.79	1.54, 1.78	0.76, 1.93	0.49, 1.96
Shiogama	0.85, 2.42	0.87, 2.21	0.89, 2.49	0.61, 2.61	0.67, 2.54	0.89, 2.29	0.60, 2.58	1.08, 2.17	1.57, 2.03	0.98, 2.32	0.75, 2.57
Natori	0.58, 1.73	0.70, 1.71	0.46, 1.75	0.35, 1.77	0.41, 1.73	0.62, 1.67	0.34, 1.82	0.84, 1.63	1.42, 1.61	0.56, 1.74	0.40, 1.76
Yamamoto	0.88, 1.84	1.60, 1.96	0.57, 1.75	0.49, 1.82	0.51, 1.76	0.84, 1.69	0.40, 1.86	1.61, 1.87	2.65, 2.28	0.70, 1.78	0.53, 1.76
10 cities & towns	0.73, 1.95	0.91, 2.02	0.63, 2.00	0.46, 2.03	0.52, 2.02	0.74, 1.82	0.48, 2.30	1.09, 1.89	1.54, 1.89	0.67, 1.98	0.53, 2.07

732

733 **Figure Captions**

734 Fig. 1 11 inversion-based source models. The sub-fault with thick lines represents the
735 asperity area, slip of which is equal to or greater than three times the average slip.

736 Fig. 2 Vertical seafloor displacements of 11 inversion-based source models.

737 Fig. 3 Overview of spectral analysis, synthesis of stochastic earthquake slips and
738 inundation mapping.

739 Fig. 4. Locations of ten cities and towns along the Sanriku coast in eastern part of the
740 Tohoku region.

741 Fig. 5 Comparison of simulated inundation depth contours in Kamaishi for the 11 slip
742 models.

743 Fig. 6 Sensitivity of inundation areas to stochastic slip variations for Kamaishi: (a)
744 inundation depth threshold = 1 m and (b) inundation depth threshold = 5 m.

745 Fig. 7 Sensitivity of K factor (a) and κ factor (b) due to stochastic slip variations for
746 Kamaishi.

747 Fig. 8 Comparison of simulated inundation depth contours in Onagawa for the 11 slip
748 models.

749 Fig. 9 Sensitivity of inundation areas to stochastic slip variations for Onagawa: (a)
750 inundation depth threshold = 1 m and (b) inundation depth threshold = 5 m.

751 Fig. 10 Sensitivity of K factor (a) and κ factor (b) due to stochastic slip variations for
752 Onagawa.

753 Fig. 11 Comparison of simulated inundation depth contours in Sendai-Natori-Iwanuma for
754 the 11 slip models.

755 Fig. 12 Sensitivity of inundation areas to stochastic slip variations for Sendai-Natori-
756 Iwanuma: (a) inundation depth threshold = 1 m and (b) inundation depth threshold
757 = 5 m.

758 Fig. 13 Sensitivity of *K* factor (a) and κ factor (b) due to stochastic slip variations for
759 Sendai-Natori-Iwanuma.
760 Fig. 14. Slip distributions and vertical seafloor displacements that correspond to 10th-,
761 50th-, and 90th-percentiles of inundated areas above 1 m depth for Kamaishi.
762 Fig. 15. Slip distributions and vertical seafloor displacements that correspond to 10th-,
763 50th-, and 90th-percentiles of inundated areas above 1 m depth for Onagawa.
764 Fig. 16. Slip distributions and vertical seafloor displacements that correspond to 10th-,
765 50th-, and 90th-percentiles of inundated areas above 1 m depth for Sendai-Natori-
766 Iwanuma.

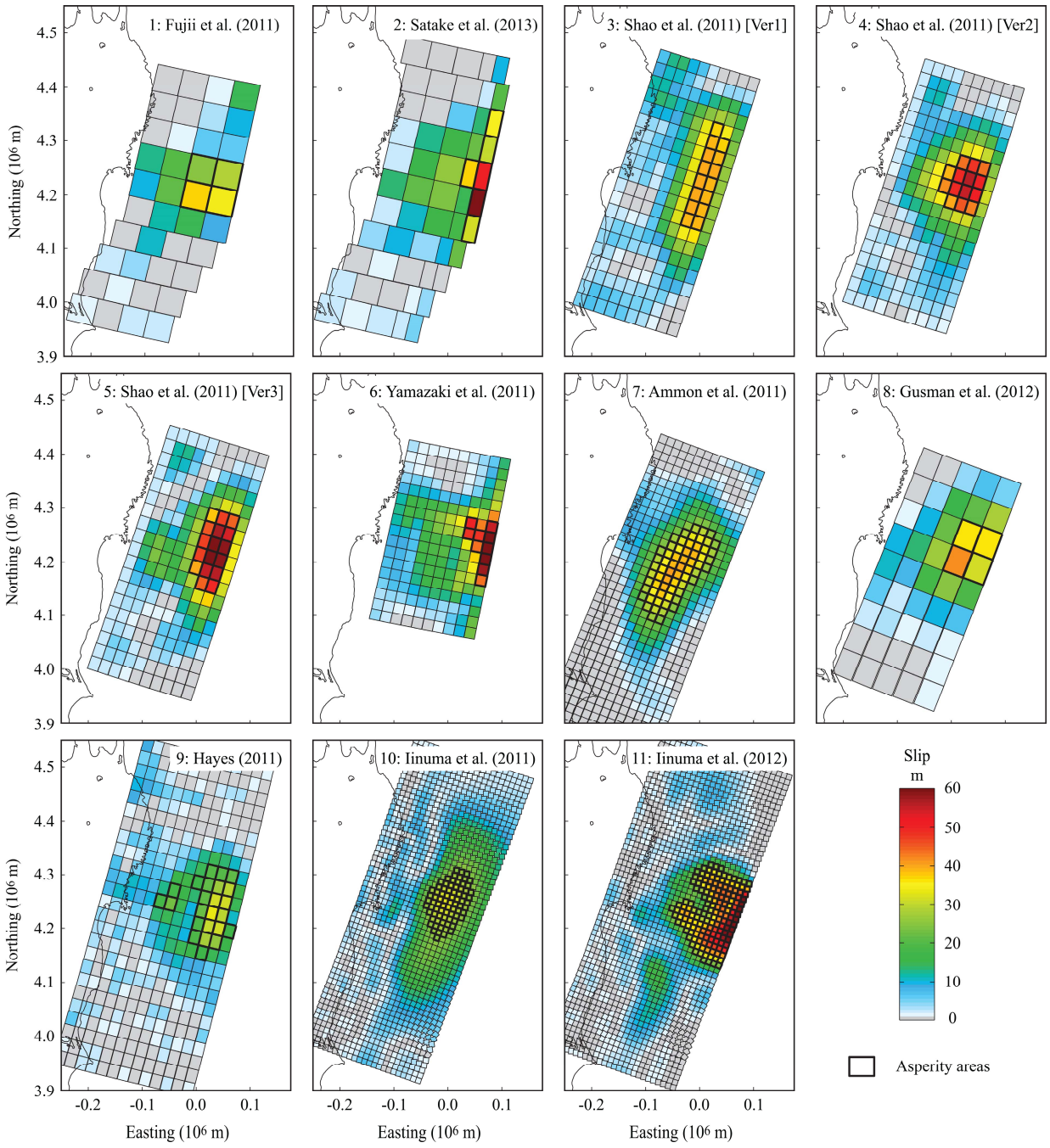

Fig. 1. Analyzed 11 inversion-based source models for the 2011 Tohoku Earthquake Tsunami. The sub-fault with thick lines represents the asperity area, slip of which is equal to or greater than three times the average slip (panels: 1-Fujii et al. (2011), 2-Satake et al. (2013), 3-Shao et al. (2011) Ver1, 4-Shao et al. (2011) Ver2, 5-Shao et al. (2011) Ver3, 6-Yamazaki et al. (2011), 7-Ammon et al. (2011), 8-Gusman et al. (2012), 9-Hayes (2011), 10-Iinuma et al. (2011), 11-Inuma et al. (2012)).

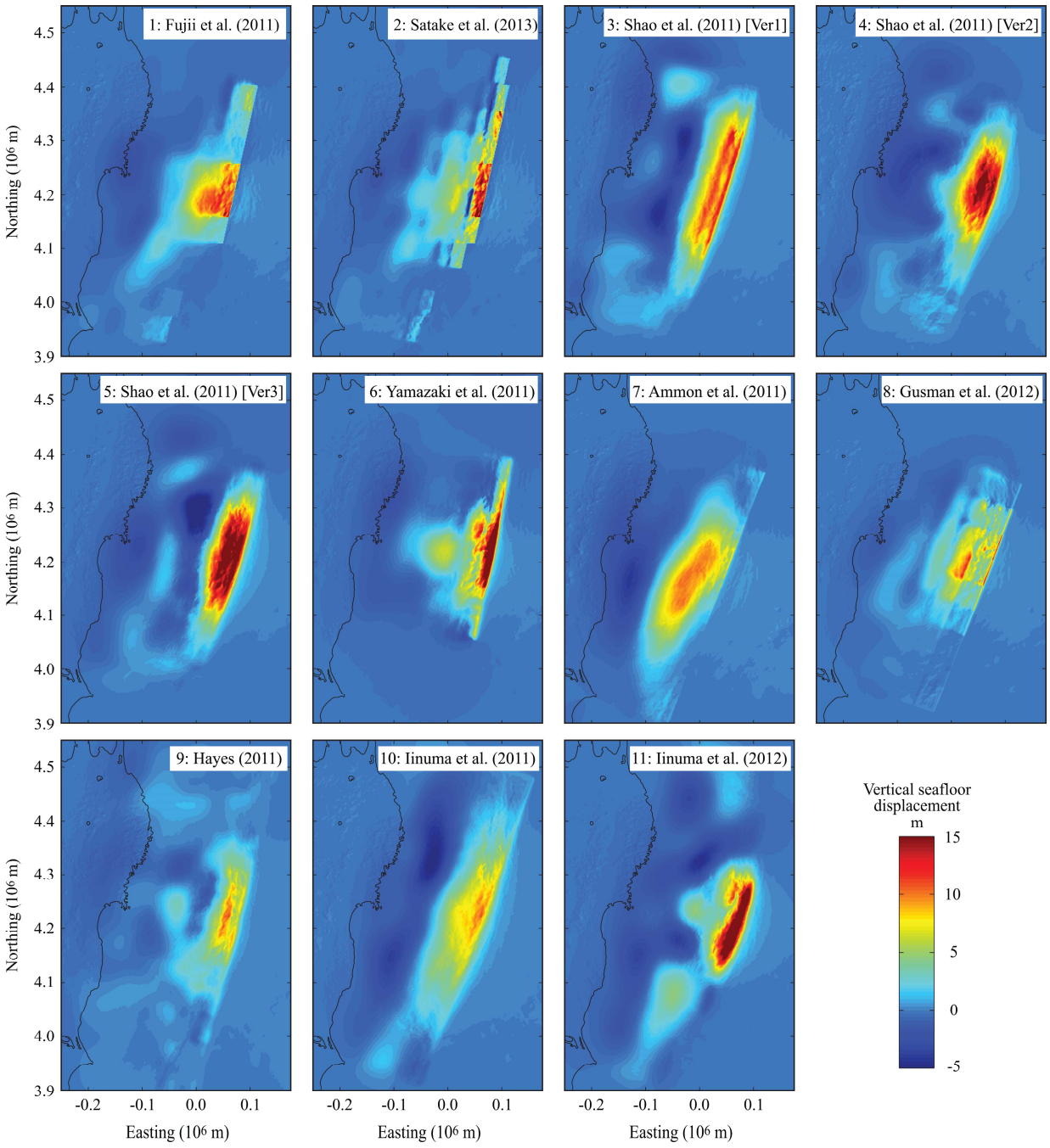

Fig. 2. Vertical seafloor displacements of 11 inversion-based source models (panel order is same to Fig.1).

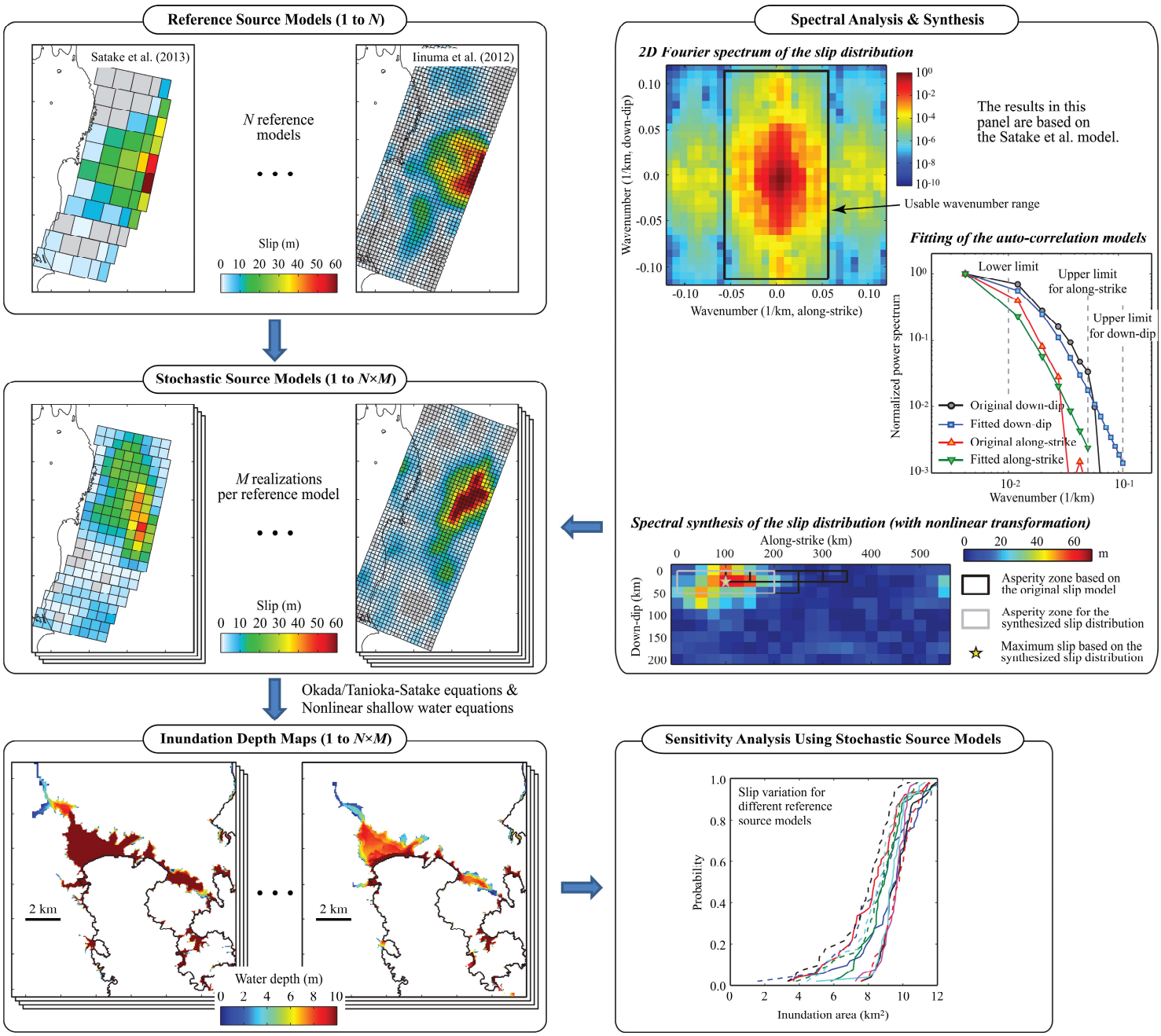

Fig. 3. Overview of flowchart of stochastic tsunami hazard assessment from spectral analysis, synthesis of stochastic earthquake slip generation, inundation mapping to sensitivity analysis of inundation.

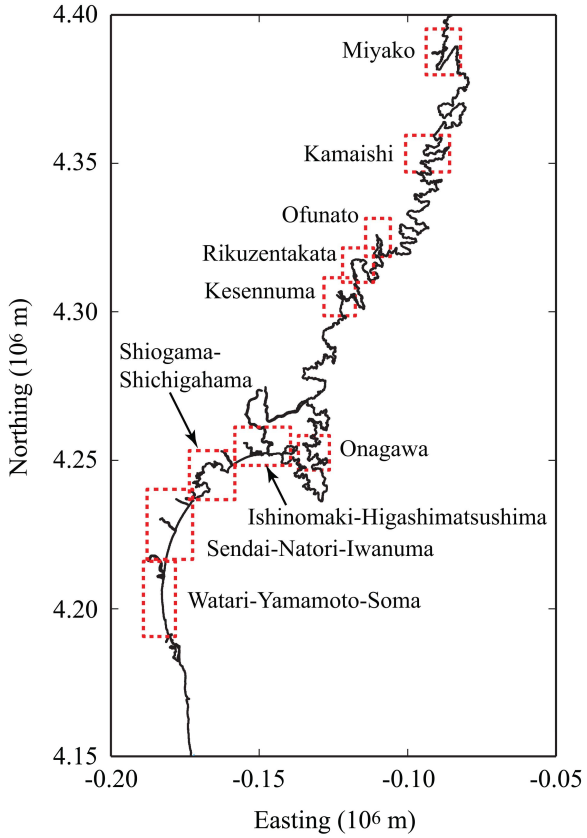

Fig. 4. Locations of reference ten cities and towns along the Sanriku coast in eastern part of the Tohoku region (boxes by dashed lines are the final nested domain for inundation simulation).

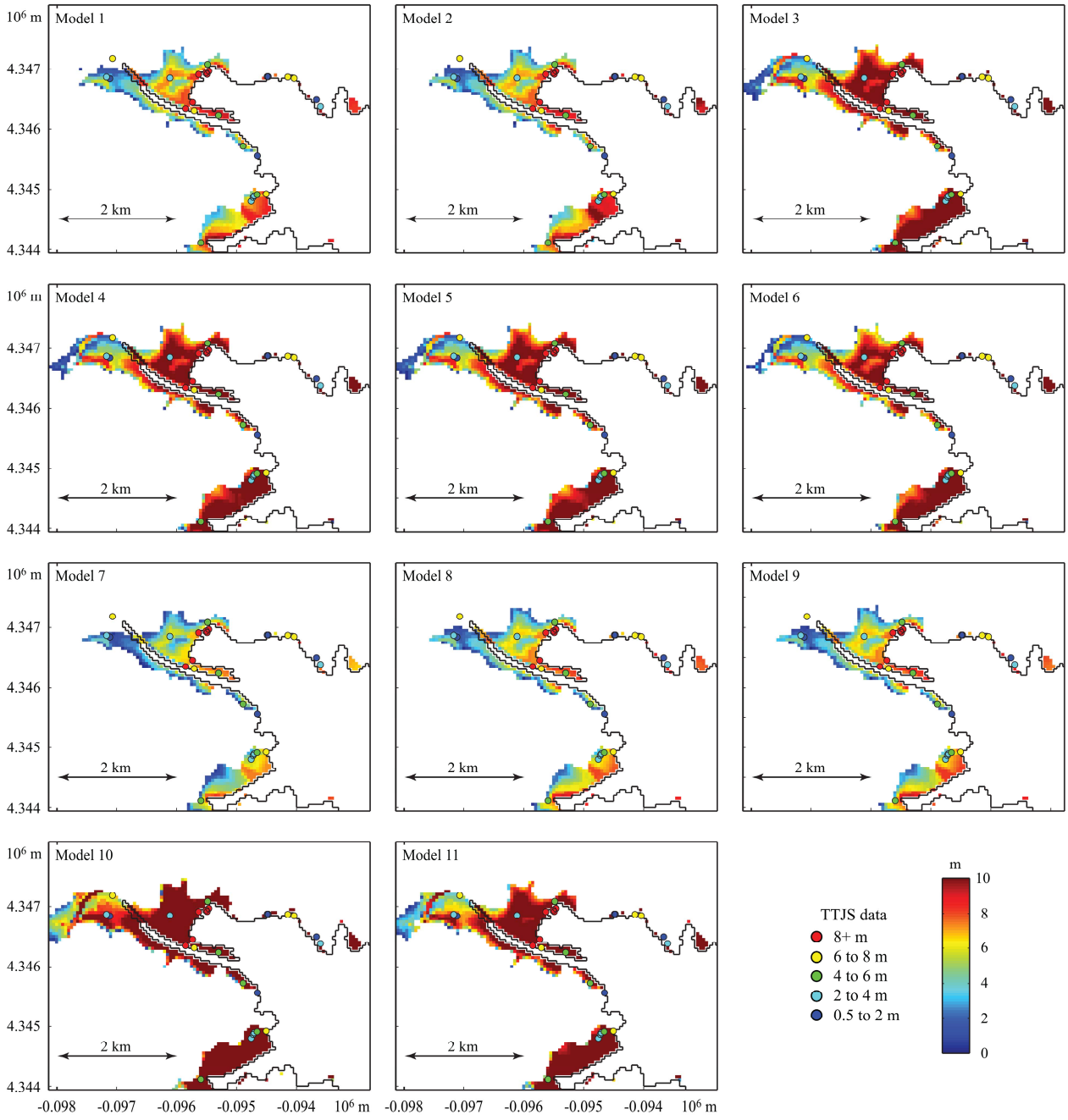

Fig. 5. Comparison of simulated inundation depth contours in Kamaishi for the 11 slip models (panel order is same to Fig.1).

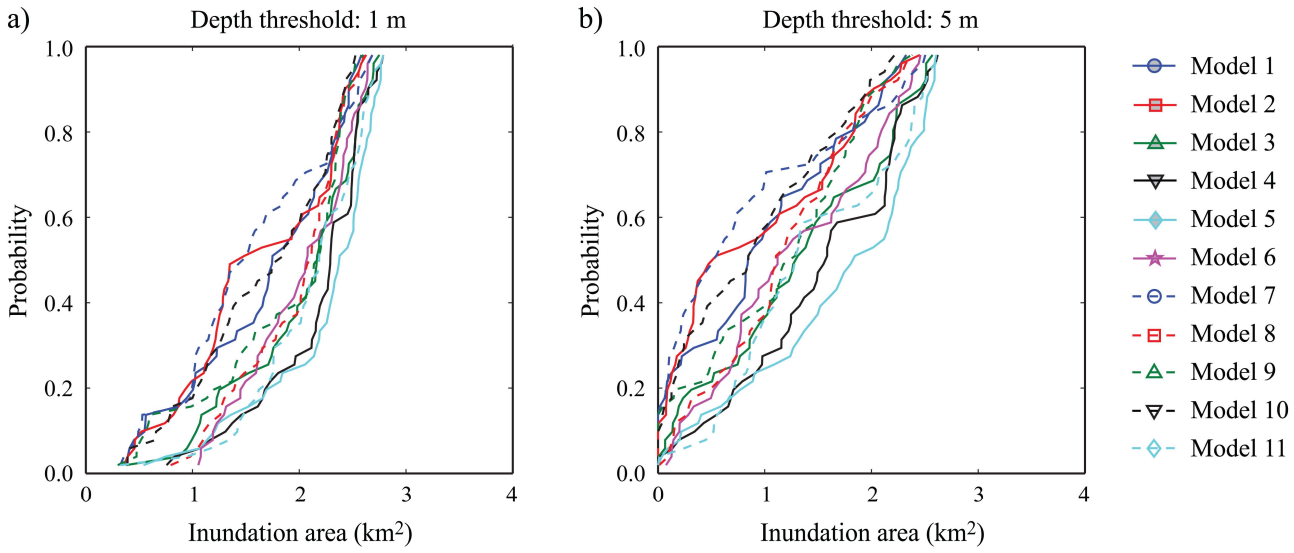

Fig. 6. Sensitivity of inundation areas to stochastic slip variations for Kamaishi: (a) inundation depth threshold = 1 m and (b) inundation depth threshold = 5 m (model 1-11 corresponds to panel order in Fig.1).

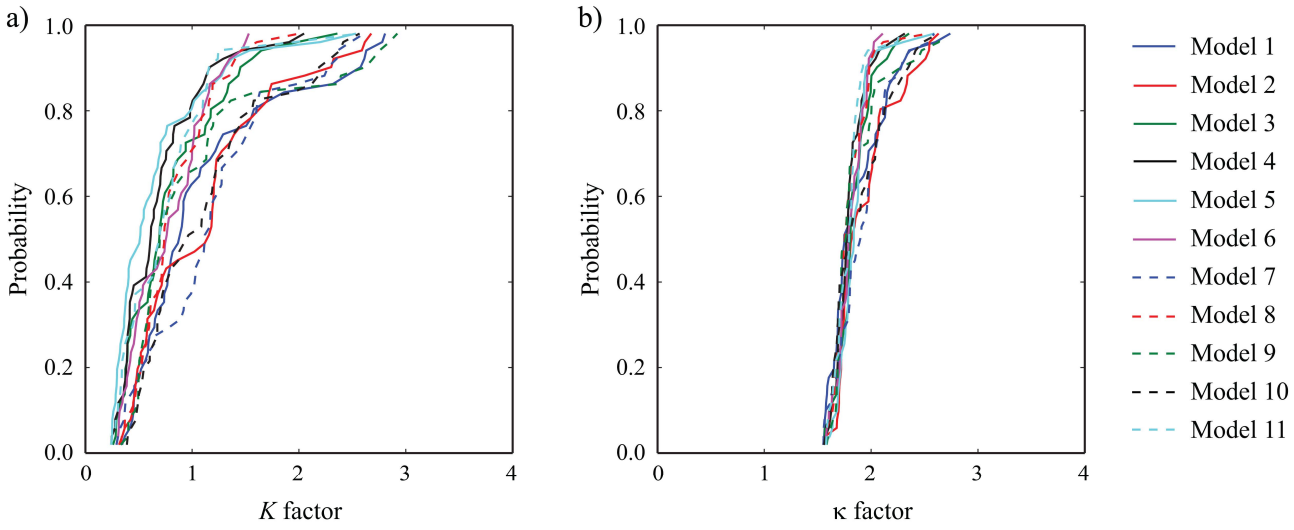

Fig. 7. Sensitivity of *K* factor (a) and κ factor (b) due to stochastic slip variations for Kamaishi (model 1-11 corresponds to panel order in Fig.1).

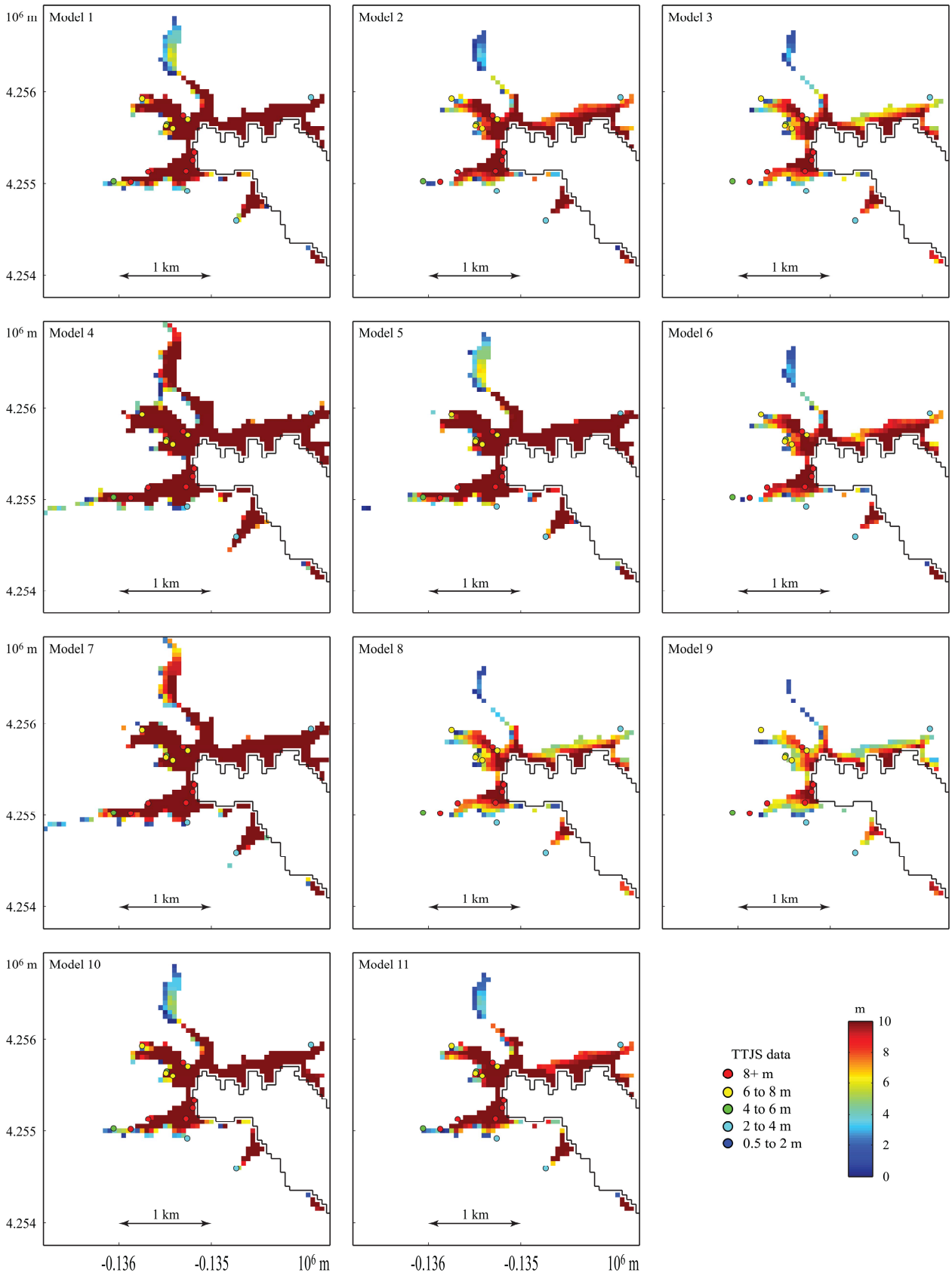

Fig. 8. Comparison of simulated inundation depth contours in Onagawa for the 11 slip models (panel order is same to Fig.1).

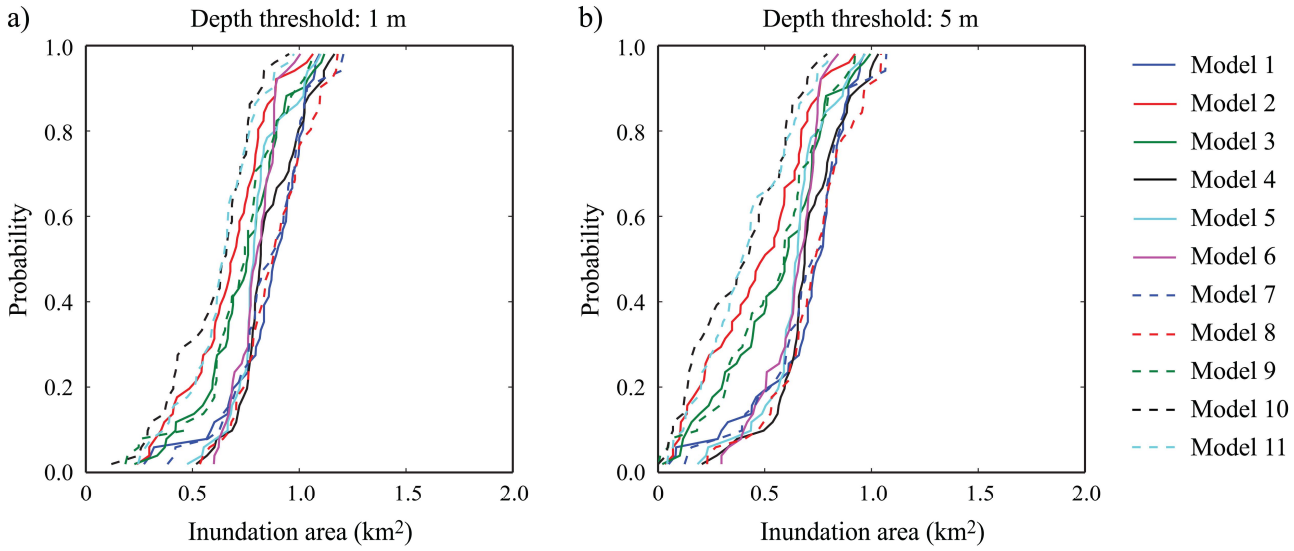

Fig. 9. Sensitivity of inundation areas to stochastic slip variations for Onagawa: (a) inundation depth threshold = 1 m and (b) inundation depth threshold = 5 m (model 1-11 corresponds to panel order in Fig.1).

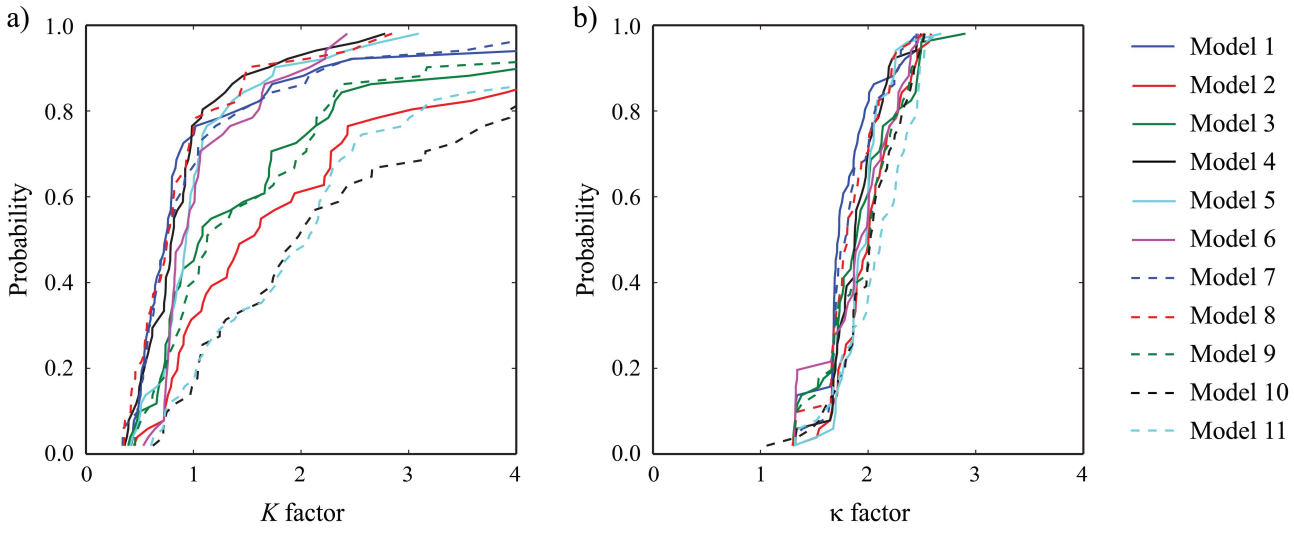

Fig. 10. Sensitivity of *K* factor (a) and κ factor (b) due to stochastic slip variations for Onagawa (model 1-11 corresponds to panel order in Fig.1).

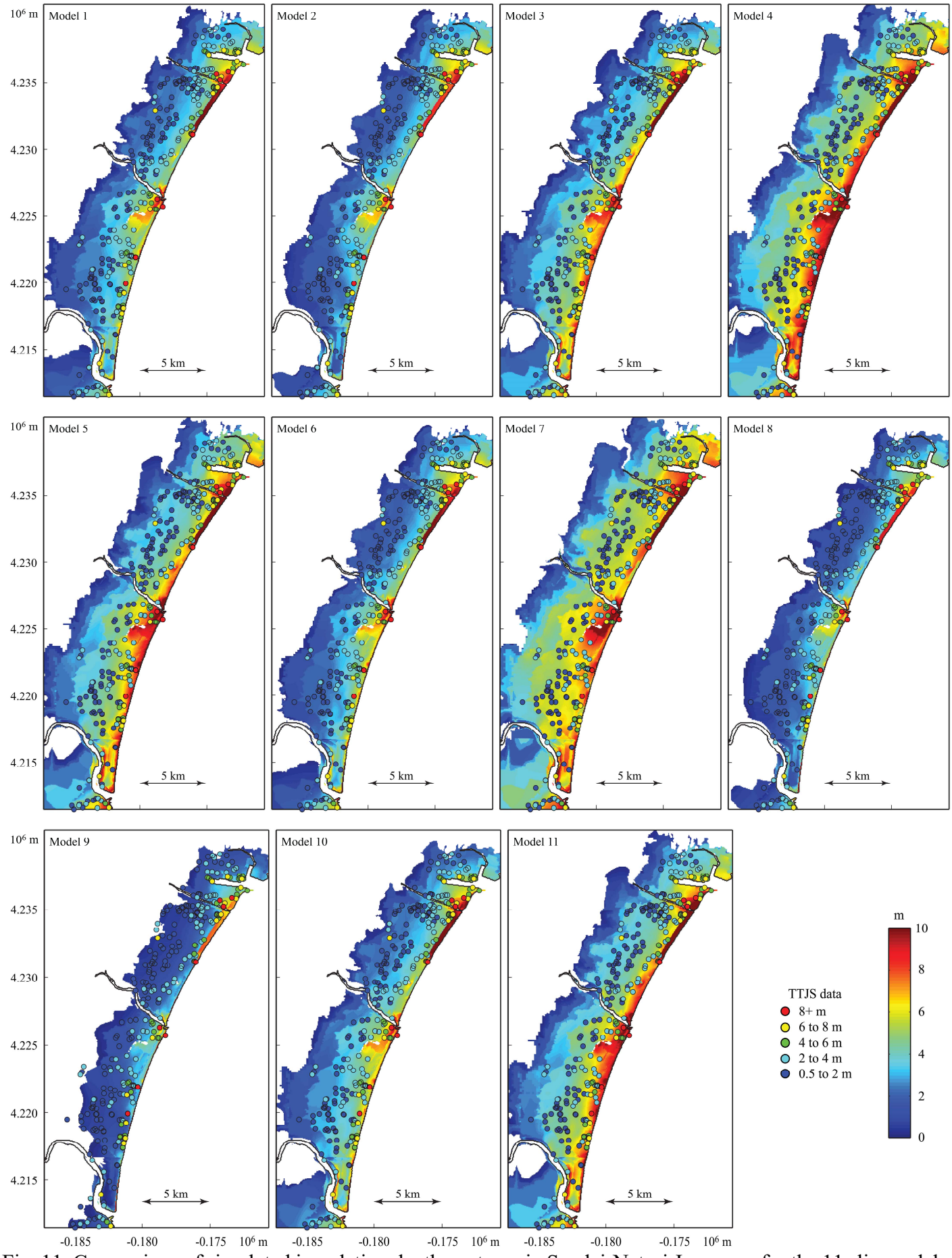

Fig. 11. Comparison of simulated inundation depth contours in Sendai-Natori-Iwanuma for the 11 slip models (panel order is same to Fig.1).

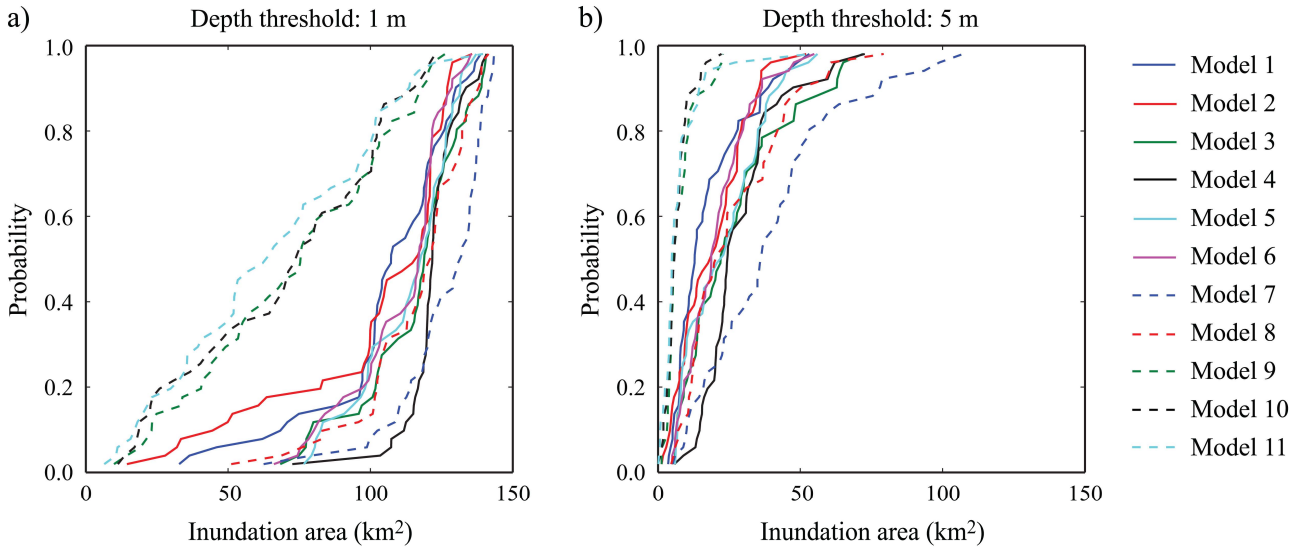

Fig. 12. Sensitivity of inundation areas to stochastic slip variations for Sendai-Natori-Iwanuma: (a) inundation depth threshold = 1 m and (b) inundation depth threshold = 5 m (model 1-11 corresponds to panel order in Fig.1).

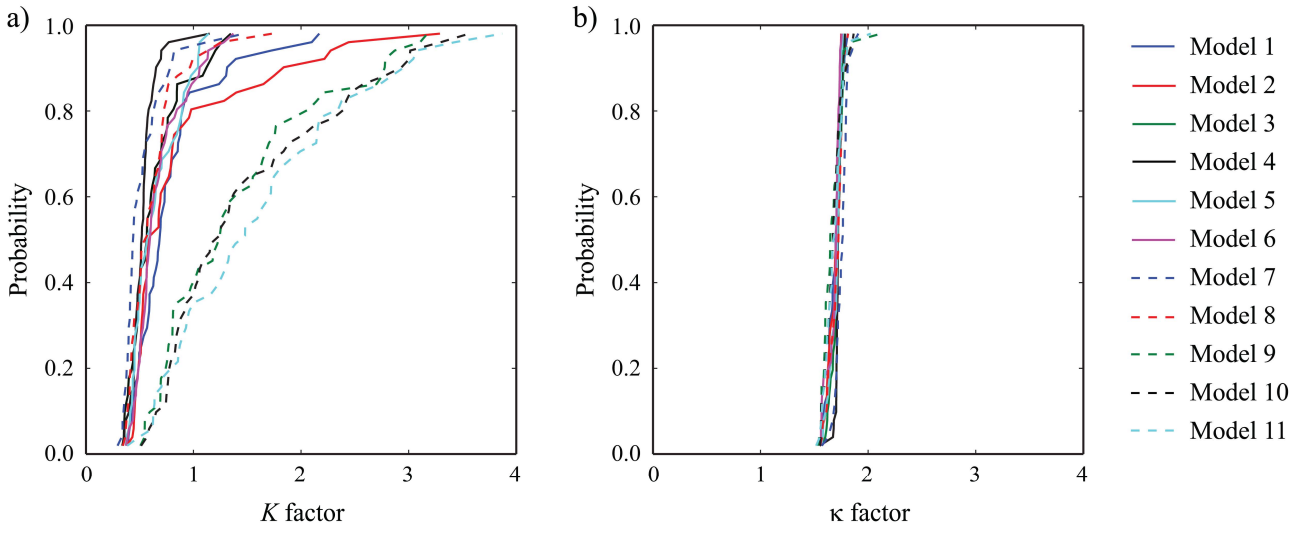

Fig. 13. Sensitivity of *K* factor (a) and κ factor (b) due to stochastic slip variations for Sendai-Natori-Iwanuma (model 1-11 corresponds to panel order in Fig.1).

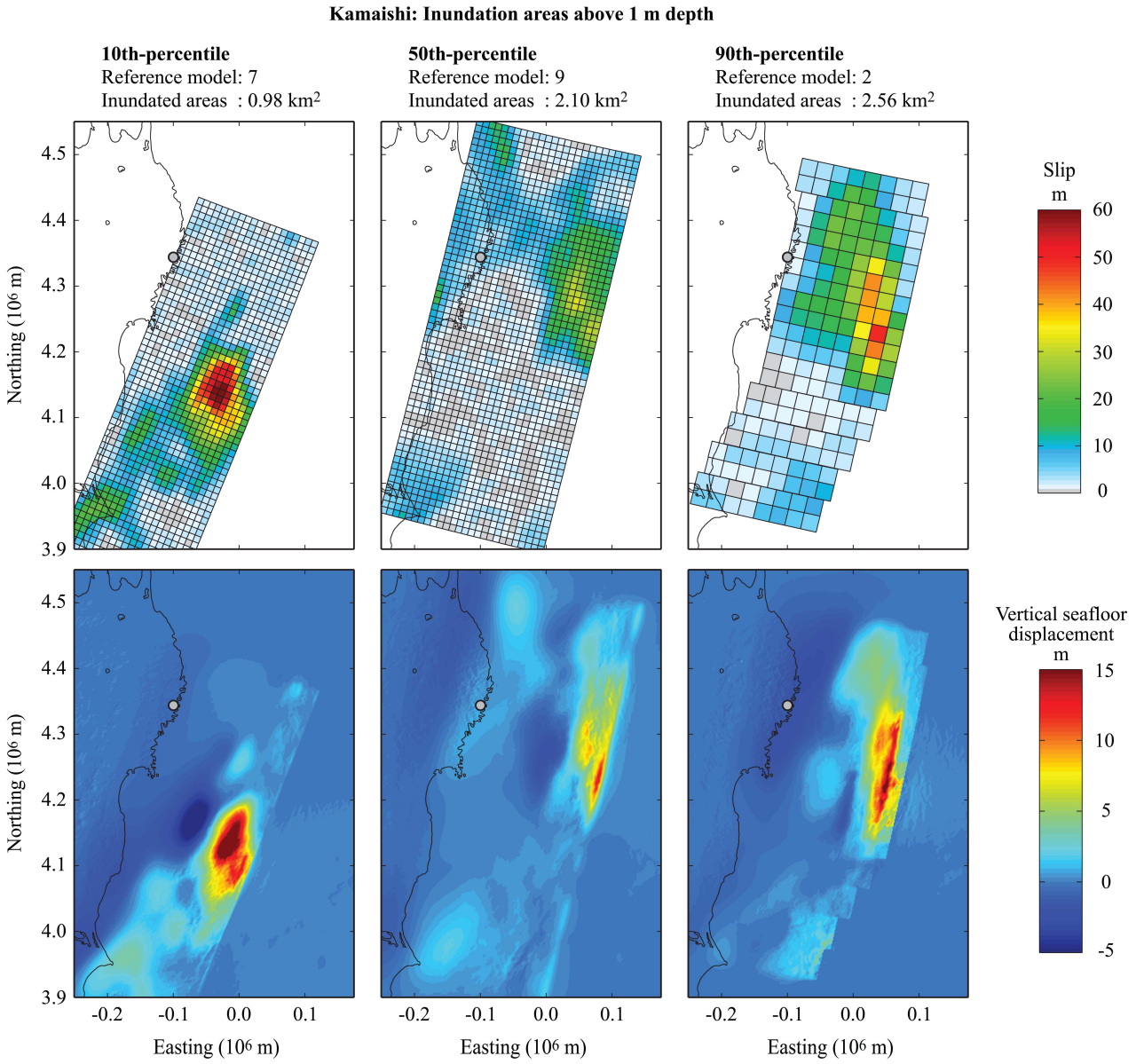

Fig. 14. Synthetic slip distributions and vertical seafloor displacements that correspond to 10th-, 50th-, and 90th-percentiles of inundated areas above 1 m depth for Kamaishi (top: slip distribution, bottom line: vertical seafloor displacement; left: 10th, middle: 50th, right: 90th).

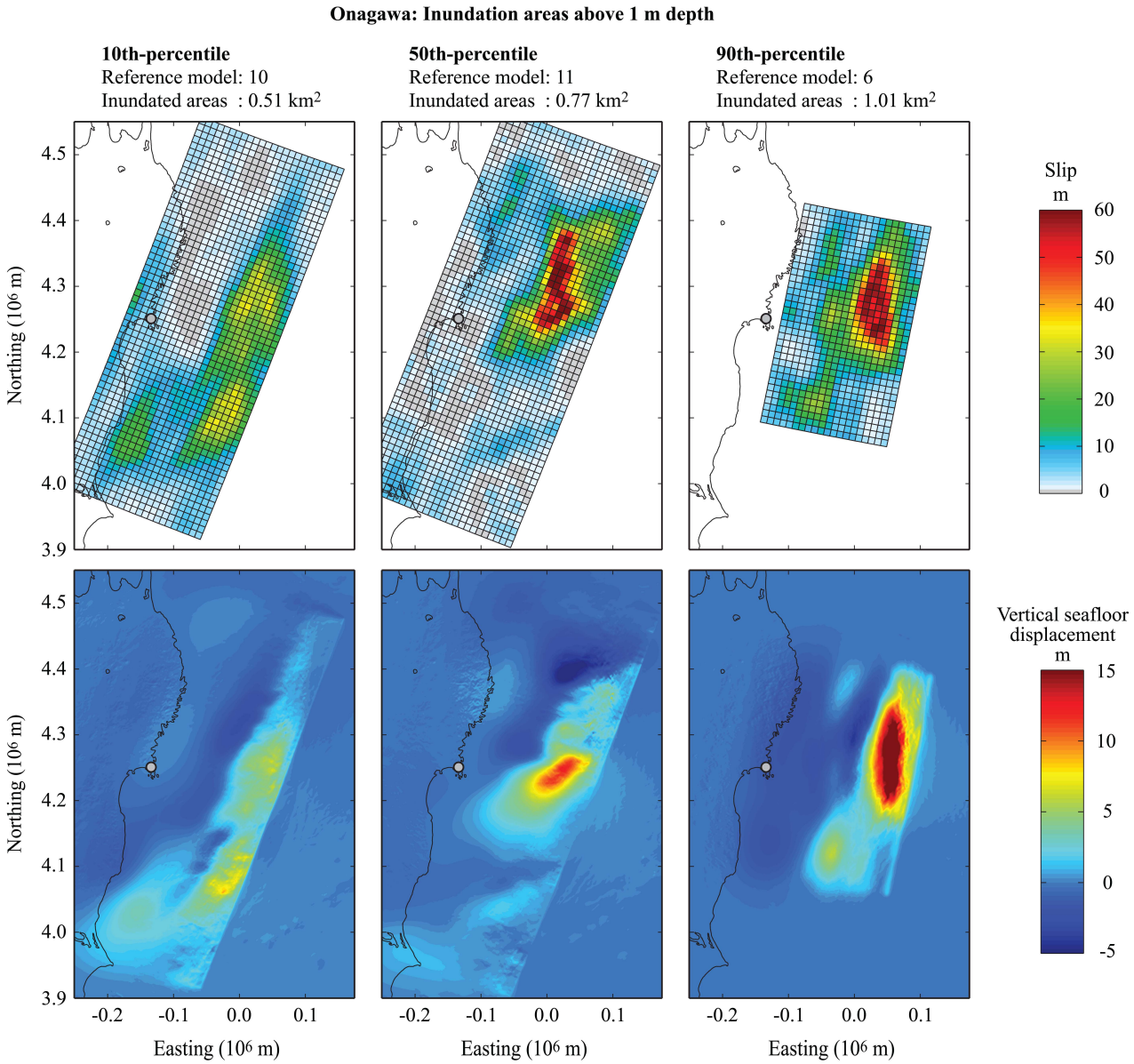

Fig. 15. Synthetic slip distributions and vertical seafloor displacements that correspond to 10th-, 50th-, and 90th-percentiles of inundated areas above 1 m depth for Onagawa (top: slip distribution, bottom line: vertical seafloor displacement; left: 10^{th}, middle: 50^{th}, right: 90th).

79

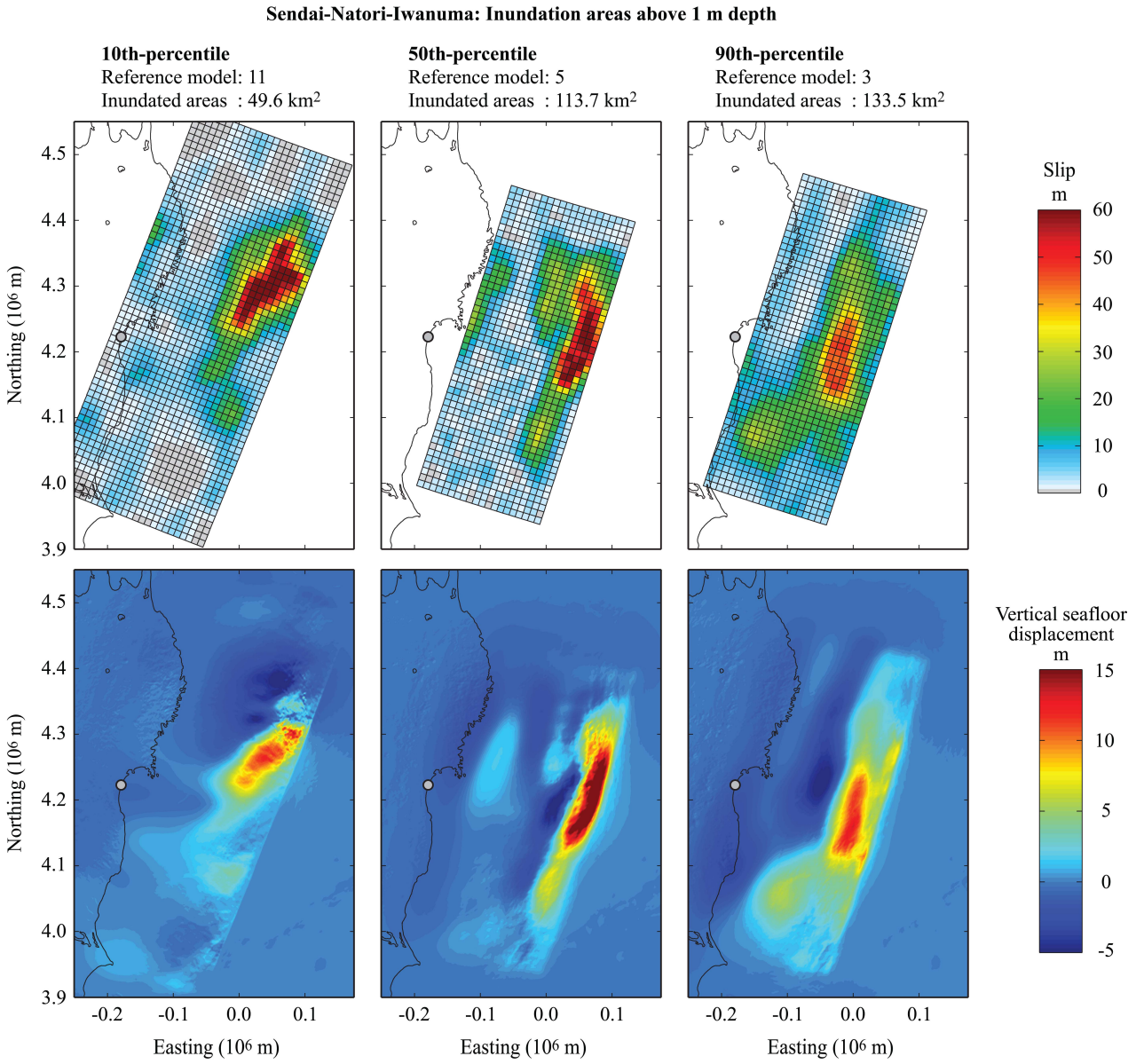

80

81 Fig. 16. Synthetic slip distributions and vertical seafloor displacements that correspond to 10th-, 50th-, and
82 90th-percentiles of inundated areas above 1 m depth for Sendai-Natori-Iwanuma (top: slip distribution, bottom
83 line: vertical seafloor displacement; left: 10th, middle: 50th, right: 90th).